GAUSSIAN BEAM TRACING

in Underwater Acoustics

Diploma Thesis

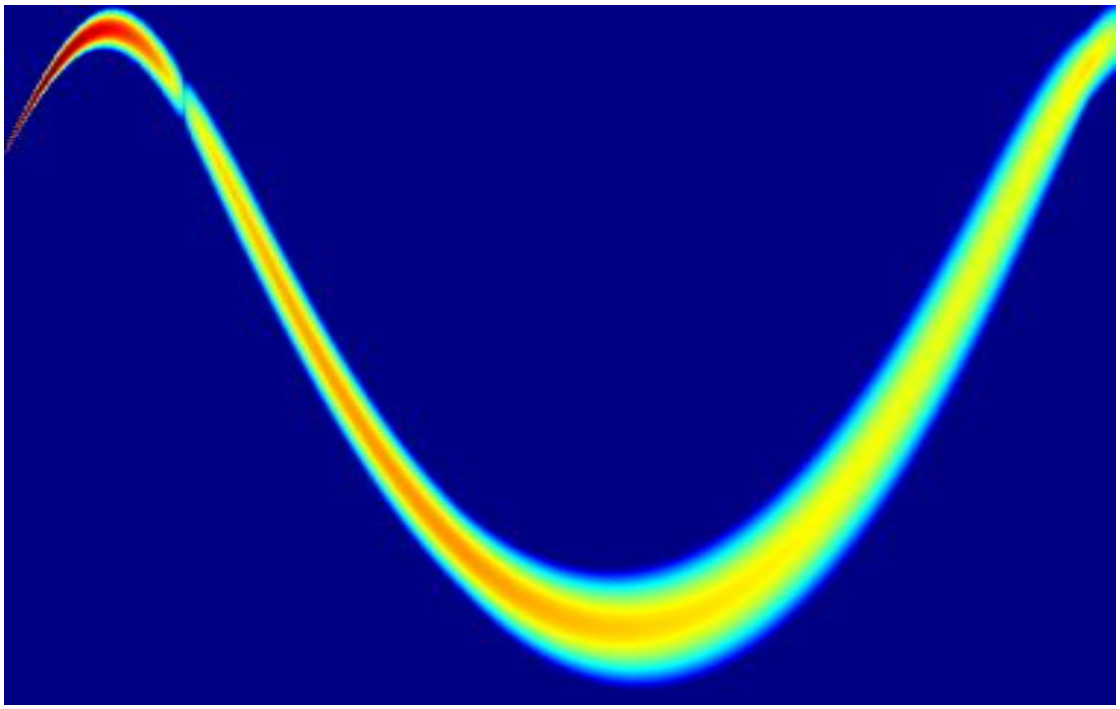

University of Crete

Student: Michail I. Sapkas, Department of Physics

Supervisor: Michael I. Taroudakis, Department of Mathematics and Applied Mathematics

Table of Contents

1 Introduction

Underwater Acoustics refers to the study of sound in water. In practice, this is done by placing hydrophones under the surface of the sea. In result, a passive listener can detect temporal variations of pressure that eventually carry information about various physical processes or human activity. Another practice is to produce sound and use it to actively acquire information, similar to turning on a flashlight in a dark room.

In contrast of electromagnetic waves, the underwater ocean environment is opaque to sound and an excellent acoustic propagating medium. In the late 80s, a lot of mathematical and computational work had been done in order to simulate sound propagation in the ocean. The fruit of this research, among others, is the ray tracing BELLHOP program, implemented by Michael B. Porter.

Some examples where the field of underwater acoustics is used in practice are: seismological research, monitoring underwater biological activity, monitoring the temperature of oceans with acoustical tomography and the weather on the surface. Some more modern topics include underwater communications and the integration of neural networks in SONAR technology. There is also a large amount of mathematical work that spans from approximate solutions to the wave equation, to statistical handling of signals, exploring chaotic behavior of rays and many more topics.

The idea of modeling waves as rays is not new. It has been thoroughly used as an effective approximation of optical light interacting with different media, as air to water refractions, and lenses. The propagation, refraction and reflection of radio waves in earth's atmosphere have been calculated and understood with ray theory. The same applies for seismic waves travelling inside the earth, in which crucial information about the earth's core and composition are revealed. Furthermore, Gaussian Beams are used in optical engineering to effectively model laser beams travelling in optical tables and interacting with equipment.

This thesis aims at presenting some general information about ray tracing modeling and its mathematical frameworks. First, the presentation of the basic concepts of underwater acoustics and modeling is in order. Afterwards, a brief heuristic approach of geometrical ray tracing will highlight the ideas and limitations of the theory and provide some initial intuition. Next, a more rigorous mathematical derivation will be presented that connects the geometrical intuition with a family of curves that are solutions of the wave equation and are normal to the wavefronts. These curves are effectively descriptions of the ray trajectories and described as a set of differential equations. I will conclude with the method of extending ray tracing applicability by converting rays to Gaussian Beams. Some computational aspects for calculating ray paths and the pressure field, and the treatment of boundaries, will be also included in the description.

By discretizing the problem into ray steps, highly complex range and depth dependence of the pressure field from the ocean waveguide can be computed with just a few basic principles, giving ray trace a computational advantage over more rigorous methods. On the other hand, ray tracing is inherently a high frequency approximation which offers its limitations. In some cases we can achieve excellent results, even in the low frequency domain, using the Gaussian Beams extension.

BELLHOP is a ray tracing program that operates by various file inputs and can output files that contain the ray paths, the pressure field and arrival times. I will benchmark BELLHOP with a normal mode program (KRAKEN) for three simple test cases and a fourth application that considers real data inputs and a more complex environment and comment on the results.

2 Basic Concepts and Modeling

Before discussing ray theory, the basic concepts and modeling principles of underwater acoustics will have to be presented. The sea environment is essentially modeled as a two-dimensional waveguide where the means of propagation is from left to right in seawater and its horizontal borders are the sea surface and the seabed.

2.1 The Wave Equation for the Acoustic Pressure

In order to describe any wave phenomenon in nature, we start by writing the wave equation for the quantity (function) obeying the wave equation. In this work we will consider the acoustic pressure as the quantity of interest. Equation $(2.1.1)$ is the wave equation for the acoustic pressure in a medium constant density. The bold $\boldsymbol{r}$ represents the vector defining the space coordinates of the point of interest in the coordinate system chosen to describe the problem and the right term an abstract forcing term that represent the source:

$$\nabla^2 p(\boldsymbol{r},t) - \frac{1}{c^2(\boldsymbol{r})}\frac{\partial^2 p(\boldsymbol{r},t)}{\partial t^2} = f(\boldsymbol{r},t) \tag{2.1.1}$$

where ∇^2 is the Laplacian operator and $c(\boldsymbol{r})$ is the sound speed.

For a point source we have that $f(\boldsymbol{r}) = A\delta(\boldsymbol{r})$. We will consider here only point harmonic sources, that is sources emitting an acoustic wave of a single angular frequency ω. Therefore, the time depended component of the sound pressure will be of the form:

$$p(\boldsymbol{r},t) = p(\boldsymbol{r})e^{-i\omega t}\,, \qquad f(\boldsymbol{r},t) = \delta(\boldsymbol{r})e^{-i\omega t}$$

Substituting into the wave equation we get a non-homogeneous second order differential equation that is independent of time and it's called the Helmholtz equation:

$$\nabla^2 p(\boldsymbol{r}) + k(\boldsymbol{r})^2 p(\boldsymbol{r}) = A\delta(\boldsymbol{r}) \tag{2.1.2}$$

where $k(\boldsymbol{r})$ is the wavenumber defined as $k(\boldsymbol{r}) \equiv \frac{\omega}{c(\boldsymbol{r})}$

The problem, as formulated above, can be solved by applying specific boundary conditions at the interfaces of the domain in which the problem is defined. The boundary conditions express continuity of pressure and the normal component of the particle velocity at the interfaces.

2.2 Solution Methods

Most solution models assume a harmonic source, effectively reducing the problem to solving the Helmholtz equation $(2.1.2)$. In this work, we will consider only environments which are axially symmetric in a cylindrical coordinate system. For this case the Laplacian operator is:

$$\nabla^2 = \frac{1}{r}\frac{\partial}{\partial r}\left(r\frac{\partial}{\partial r}\right) + \frac{\partial^2}{\partial^2 z}$$

and the point harmonic source is located at range $r = 0$ and depth z_s .

2.2.1 Wavenumber Integration

Assuming a range – independent environment, that is an environment whose parameters don't change with respect to range, the Helmholtz equation can be separated into depth and range equations (Jensen et al. 2011):

$$\frac{d^2}{dz^2}p(k_r,z) + \left(k^2 - {k_r}^2\right)p(k_r,z) = A\delta(z - z_s) \qquad (2.2.1.1)$$

and:

$$p(r,z) = \int_0^\infty p(k_r,z)J_0(k_r,z)\,k_r\,dk_r \qquad (2.2.1.2)$$

$p(k_r,z)$ is the solution to the differential equation $(2.2.1.1)$ for a given horizontal component of the wave vector which is also the separation constant, k_r . A is the source amplitude. J_0 is the Bessel function of the first kind of zero order.

The wavenumber integration method refers to numerically solve equation $(2.2.1.2)$ for various values of k_r and then proceed to numerical integrate equation $(2.2.1.1)$.

2.2.2 Normal Modes

The Normal Mode solution is based on the series expansion of the acoustic pressure over a set of eigenfunctions $Z_n(z,r)$ defined at each range of the environment. The eigenfunctions are solutions of the so called "depth problem" which is defined through the differential equation $(2.2.2.1)$ at each range r, supplemented by the appropriate boundary conditions.

$$\frac{\partial}{\partial z}\left[\frac{1}{\rho(z,r)}\frac{\partial Z_n(z,r)}{\partial z}\right] + \left[\frac{k^2(z,r)}{\rho(z,r)} - \frac{\lambda_n(r)}{\rho(z,r)}\right]Z_n(z,r) = 0 \qquad (2.2.2.1)$$

Note that in this equation we have introduced the density ρ of the medium to account for the density differences of the medium subdomains. $\lambda_n(r)$ are the eigenvalues of the depth problem. The acoustic pressure is then given by equation:

$$p(r,z) = \sum_{n=1}^{N} R_n(r)Z_n(z,r) \qquad (2.2.2.2)$$

where N is the maximum number of modes considered, in order that the series expansion converges to a stable solution.

Note that $\sqrt{\lambda_n(r)}$ is the horizontal component of the wavenumber corresponding to mode n and it is usually referred as k_{rn} .

For a range independent environment considering the Sommerfeld radiation condition and the source excitation function defined in this axially symmetric environment to be $-\frac{1}{2\pi r}(z - z_s)$ the range function $R_n(r)$ is shown to be of the form:

$$R_n(r) = \frac{i}{4\rho(z_s)}H_0^{(1)}(k_n\,r)Z_n(z_s) \qquad (2.2.2.3)$$

where z_s is the depth of the source, $H_0^{(1)}$ is the Hankel function of zero order and first kind and the eigenvalues are not anymore r-depended.

Thus, the acoustic pressure takes the form:

$$p(r,z) = \frac{i}{4\rho(z_s)} \sum_{n=1}^{N} Z_n(z_s) Z_n(z) H_0^{(1)}(k_n r) \qquad (2.2.2.4)$$

More complicated environments (e.g. range-depended environments) can also be solved using the Normal Mode theory (see Jensen et al. 2011).

2.2.3 Parabolic Equation

We assume a solution in the form of a cylindrical outgoing wave:

$$p(r,z) = \Psi(r,z) H_0^{(1)}(k_0 r) \qquad (2.2.3.1)$$

By imposing a paraxial approximation $\frac{\partial^2 \Psi}{\partial r^2} \ll 2ik_0 \frac{\partial \Psi}{\partial r}$, the Helmholtz equation becomes:

$$2ik_0 \frac{\partial \Psi}{\partial r} + \frac{\partial^2 \Psi}{\partial z^2} + \left(k^2(z) - {k_0}^2\right)\Psi = 0 \qquad (2.2.3.2)$$

We can now factor the depth operator, which we will denote as Q, and keep only outgoing terms:

$$\frac{\partial p}{\partial r} = ik_0\sqrt{(1+Q)}\, p \quad (2.2.3.3), \qquad Q \equiv \frac{1}{k_0}\left(\frac{\partial^2}{\partial z^2} + k^2(z) - {k_0}^2\right) \quad (2.2.3.4)$$

The parabolic equation method works by approximating the square root containing the depth operator $\sqrt{(1+Q)}$ with a Padé series expansion and then range – march the solution of the pressure field:

$$p(r+\Delta r, z) = p(r,z) \cdot e^{ik_0 \Delta r} \cdot \left(1 + \sum_{j=1}^{m} \frac{a_{j,m} Q}{1 + b_{j,m} Q}\right) \qquad (2.2.3.5)$$

2.2.4 Ray Methods

For the ray methods we assume that the amplitude and the phase are slowly varying functions of position, along a particular ray. This is inherently a high frequency approximation which can be used as justification to separate of the two functions. Further explaining the theory and concept behind this solution method is the main subject of this thesis.

2.3 The Oceanic Medium

Figure 2-1 below presents the oceanic environment in cylindrical coordinate system with axial symmetry. The source is considered at the point $(0, z_s)$ and the location of the point of interest (measuring point) at (R, z).

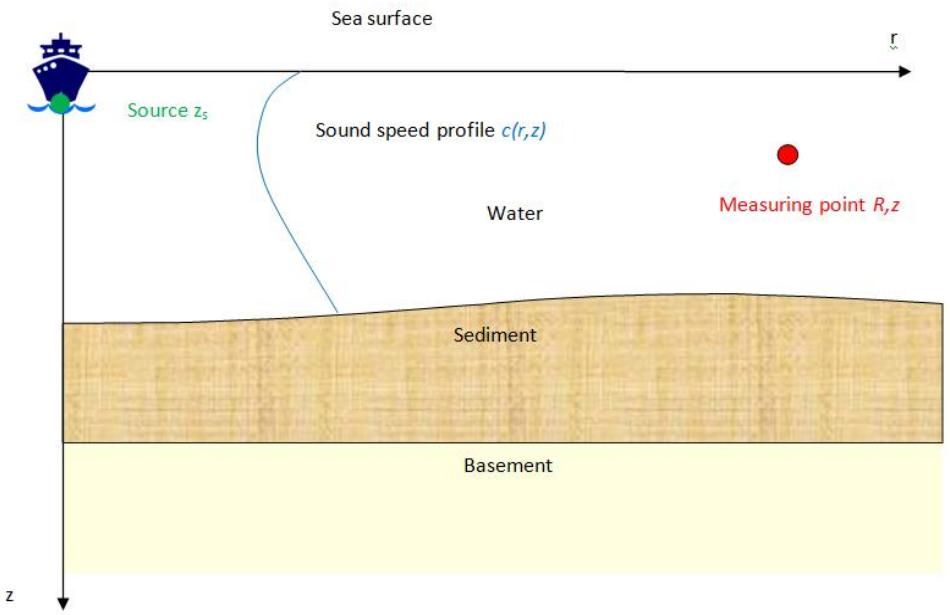

Figure 2-1 The oceanic 2-D waveguide

Seawater is modeled with density $\rho = 1 \frac{gr}{m^3}$. As sound travels, it weakly interacts with the medium. The result of this interaction is the conversion of acoustic energy into heat, which means that there is a very small energy leakage proportional to the distance. This interaction is completely ignored in this thesis, although some propagation models (such as BELLHOP) can account for it.

Some additional notes on the acoustic sources, the sound speed profile and the medium interfaces will be given in the subsequent sections.

2.4 The Source

There are many potential sources of acoustic waves in the ocean. From manmade speaker arrays to biological or seismic activity, the underwater environment is filled with impulsive or continuous sounds and ambient noise. Figure 2.1 above indicate a ship as the source of sound in the environment.

The source, in this ray trace model, is just a user specified point in space that produces continuous sound at a user specified frequency and it serves as the initial launch point of all rays.

2.5 The Surface of the Sea

The sea surface could be covered in floating ice with complex underwater structure or could be large swell waves that morph the air – water boundary (the existence of bubbles also complicate things).

The huge density difference between water and air consist a boundary that fully reflects the sound waves that hit on it (pressure release). Therefore, the air – water interface is modeled as an acoustic "mirror". Standard modeling techniques consider the sea surface as flat and possibly allow the user to specify a “roughness” coefficient that tries to mimic some amount of random scattering. For the sake of simplicity, we will consider the sea surface as flat and pressure release.

2.6 The Bottom

The bottom can affect acoustic propagation in two ways: its composition and its geometry (bathymetry).

In the initial layers, the bottom is usually composed of soft materials (mud, clay, sand) and in the deeper layers it transits to a rocky bottom. In contrast to the surface, because the density of the materials does not change dramatically, when the acoustic wave strikes the water-bottom interface, some of the energy is reflected and a percentage penetrates to the bottom. Fluid layers allow the propagation of longitudinal (acoustic) waves only. They are often defined as acoustic layers. Elastic layers allow propagation of shear waves as well. (Mixtures of elastic and acoustic layers with possible sound speed gradients, attenuation and density are all exactly represented by a complex reflection coefficient. Nevertheless, one can still do a reasonable job of treating complicated layered bottoms through a tabulated reflection coefficient. If the bottom supports the propagation of shear waves then some of the energy will be converted into propagating shear waves. In addition, the process of energy loss due to diffusion into the bottom can be described with the introduction of an attenuation constant. In shallow seas, sound waves can reflect of the seabed several times and thus weaken rapidly.

The above simple example shows how the geometry of the seabed plays an important role. Other geometric characteristics that can affect the propagation of sound are mounts and trenches. These vertical or sloping structures reflect waves at angles beyond the simple horizontal plane and directly affect the acoustic field. In addition, sound can enter these bottom structures, get refracted and potentially be reinserted back into the marine environment.

So it’s obvious that the existence of an elastic bottom with some complex geometry, greatly complicates the problem of simulating sound propagation, and therefore the final field of pressure. How the computational model handles bathymetry is a key factor and defines limitations, advantages and disadvantages.

2.7 The Speed of Sound

Perhaps the most important factor of acoustic propagation is the speed of sound. The sound speed varies with depth and range. For each range in the oceanic waveguide the speed of sound is a function of depth and a sound speed profile (SSP) is defined. The profile may be derived by direct measurements in the field using an empirical formula which links the speed of sound with temperature, salinity and pressure (or depth), namely: $c = c\ (T, S, p)$.

The sound speed profile is seasonally variable in the first hundreds of meters and can be affected by tides and currents. At greater depths it usually remains constant as it is not affected by the seasons

or surface conditions and the low temperature combined with the high pressure give it an increasing gradient.

So if we know T, S, p we can construct a velocity function $c = c(r, z)$ that relates a velocity to any point in the coordinate system. Although most of the acoustic propagation models including BELLHOP, which is the basic model used in our work, can manage range depended sound speed profiles, we will use speed profiles that depend only on depth. That is, in a column of water from the surface to the bottom, sound waves perceive a fixed velocity profile $= c(z)$.

Obviously, even with this simplification, the value of c depends on the depth. This variation of the speed of sound in each depth creates refraction effects resulting in curving of the sound energy towards areas where the speed of sound becomes minimal. If the curve $c(z)$ has a minimum (that is $\frac{dc}{dz} = 0$), sound tends to get "trapped" and continues to propagate for extremely long distances without losing energy. This phenomenon is quite common in real applications and the depth this happens is referred to as the *acoustical channel* (e.g. the SOFAR channel).

Since the SSP is given in pairs of depth-range and sound speed, the proper interpolation when tracing the ray paths, must be selected.

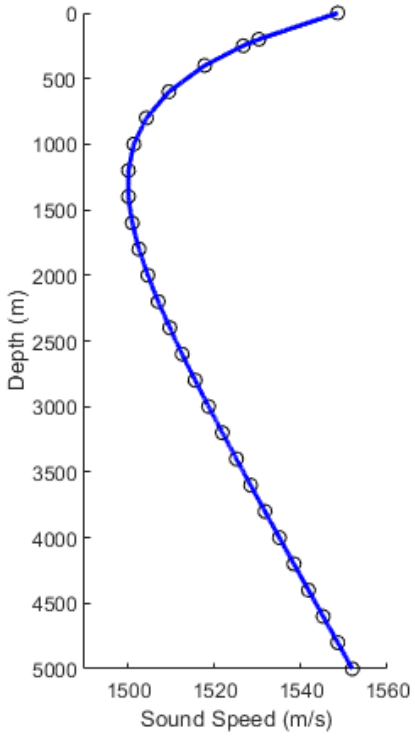

Figure 2-2 The Munk Sound Speed Profile

2.8 Sound Intensity

Intensity is the average rate of flow of energy through a unit area that is normal to the direction of propagation. The magnitude of the intensity of a plane wave at a specified position is:

$$I = \frac{p_{rms}^2}{\rho c}$$

2.9 Decibel Units

When we measure sound, we effectively measure pressure. *Sound pressure* or *acoustic pressure* is the local pressure deviation from the ambient (average or equilibrium), caused by a sound wave. The pressure wave is measured in *decibels* (dB) which is defined as the logarithmic ratio of intensities. Therefore absolute sound pressure levels can be expressed by introducing a reference intensity of a plane wave having a root mean squared (*rms*) pressure of $0\ dB$ when $p_{rms} = 1\mu Pa$.

2.10 Transmission Loss

The intensity of the acoustic field obviously changes as the acoustic wave propagates in the oceanic waveguide. The standard measure in underwater acoustics of the change of acoustic signal strength with range is called *Transmission Loss* and is defined as:

$$TL_{12} = -10\log\frac{I(r_2, z_2)}{I(r_1, z_1)} = -20\log\frac{|p(r_2, z_2)|}{|p(r_1, z_1)|}$$

When r_2 is assumed to be greater than r_1 the acoustic intensity at point 2 is less that in point 1 due to geometrical spreading and the minus in the expression results positive results.

It is customary to refer to the transmission loss with reference to a distance of 1 m from the point source, in which case the TL gives an indirect quantification of the acoustic field. The corresponding intensity and pressure field are indicated as I_0 and p_0 correspondingly.

$$TL = -10\log\frac{I(r, z)}{I_0} = -20\log\frac{|p(r, z)|}{|p_0|} \qquad (5.4.1)$$

$$reference\ (I_0, p_0)\ dB\ at\ 1m\ distance\ from\ the\ source$$

The representation of the acoustic field using Transmission Loss instead of pressure is preferred in the community for practical reasons. First, the fluctuations of pressure can be large compared to the initial intensity. Second, by plotting Transmission Loss, we can easily refer to losses for any pressure amplitude p_0 we are given, effectively generalizing our results.

In general, main acoustic loss mechanisms are the *geometrical spreading loss*, which relates to the geometry of the problem, and loss due to attenuation from boundary interaction (see 7.3 *Bottom Loss*). Transmission loss may be considered to be the sum of all these mechanisms.

3 Ray Theory

In this section, a simple ray model is introduced before the more rigorous description. This simple description will highlight the strengths and weaknesses of the ray approximation and it is helpful to develop an initial intuition. An acoustic ray is defined as the curve in each point of which the wavenumber vector is tangent. Rays can also be considered as normals to the pressure wavefront generated by the source (Figure 3-1).

3.1 A simple Ray Trace Recipe

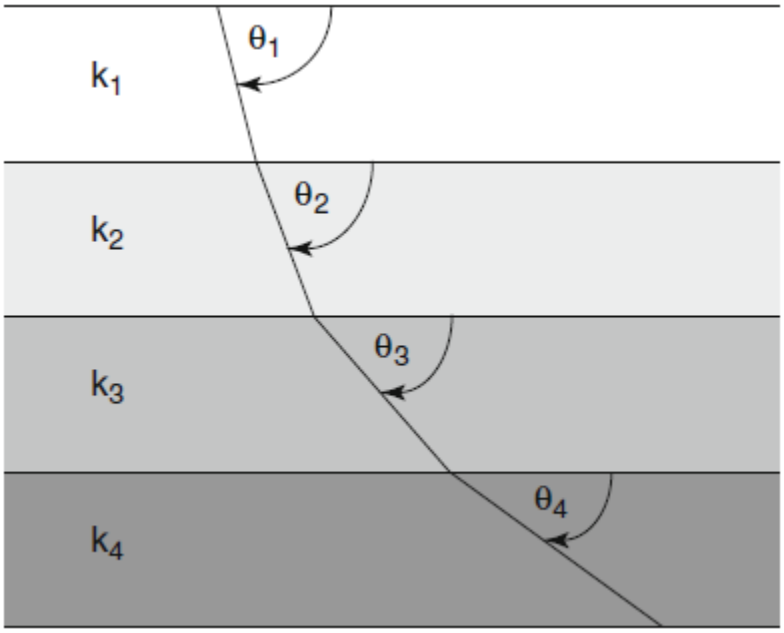

Figure 3-1 Stratified Medium

We begin by modeling the ocean environment as a horizontally stratified medium. The given sound speed profile $c(z)$ is discretized by means of horizontal layers in each one of which the sound speed is constant. We can compute the path of a ray, in terms of discreet sequential positions, given the initial conditions of the ray and using Snell's law. The initial conditions refer to knowing the initial position and launch (emission) angle of the ray.

Let's assume the ray starts at position $\boldsymbol{r}_{source} = (r_s, z_s)$ with an angle from the horizontal axis θ_0 and it happens to be located in layer i. Applying Snell's law when the ray steps from layer i to layer j we get:

$$\frac{\cos(\theta_0)}{c_i} = \frac{\cos(\theta_j)}{c_j}$$

If we envision a fluid with continuous varying sound speed and letting the thickness of each layer to be dz we can write:

$$\frac{\cos(\theta_0)}{c(z_s)} = \alpha = \frac{\cos(\theta_i)}{c(z_i)} = \ldots = \frac{\cos(\theta_f)}{c(z_f)}$$

Furthermore, if we observe that the fraction $\frac{\cos(\theta_0)}{c(z_s)} = \alpha$ is a constant defined by the initial conditions, then we can conclude that at any point of its path, this particular ray must conserve this quantity. Therefore, we immediately acquire a simple computational scheme to trace a ray. The next launch angle of the ray can easily be found by solving for θ_f:

$$\theta_f = \cos^{-1}\big(\alpha \cdot c(z_f)\big) \tag{3.1.1}$$

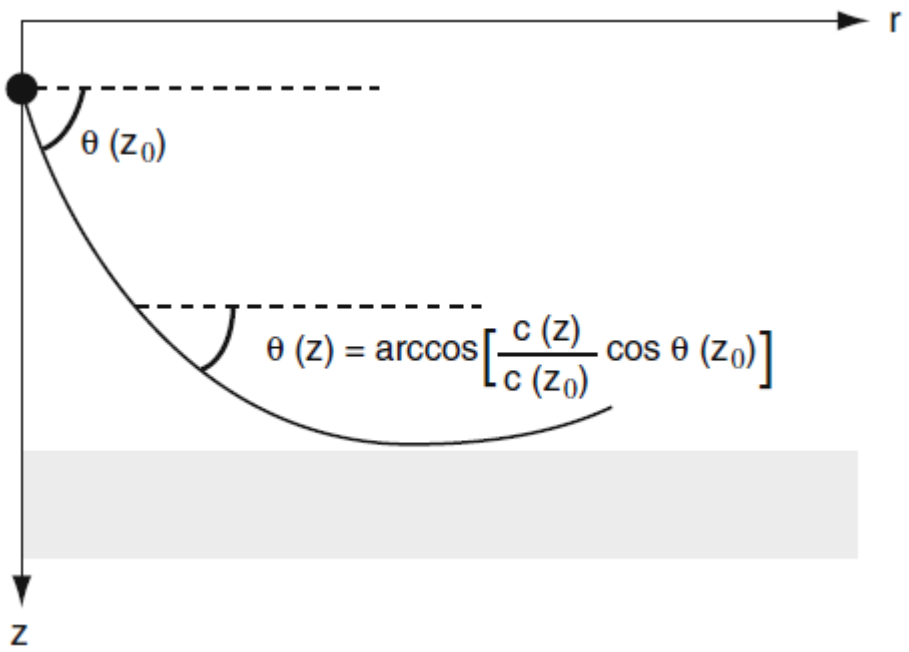

Figure 3-2

The constant α is also refered to as the *waveguide invariant*.

The actual trajectory of the ray, is computed by discretizing a step towards the horizontal axis dr, the depth axis dz, or a step towards the tangent of the ray ds. All these coordinates are connected with each other by simple geometry:

$$ds = \frac{dr}{\cos(\theta_i)} \tag{3.1.2}$$

$$ds = \frac{dz}{\sin(\theta_i)} \tag{3.1.3}$$

We can also keep track of the phase of each ray expressed as distance traveled over velocity, which basically is the ray flight time if we integrate:

$$d\tau(s) = \frac{ds}{c(z_f)} \tag{3.1.3}$$

As we track the ray it is possible that it encounters the boundary surface or the bottom. The surface is a perfect reflector, bouncing the ray back at the same angle it hit. At the bottom, Snell's law is in effect and the reflected ray comes with an attenuation cost of Bottom Loss.

3.2 Geometrical Spreading of Acoustic Power

In two dimensions we can visualize a ray tube of constant power that emanates from the source. We can calculate the Transmission Loss at the ray tube by considering the relation of the acoustic pressure between the initial power P_o and the power at any point $P(r)$.

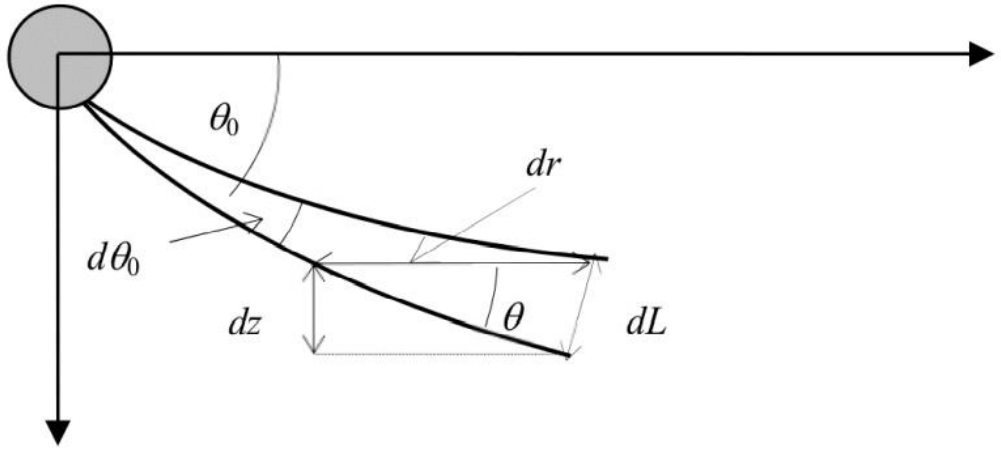

Figure 3-3

The intensity at each point in the ray tube is the ratio of the power carried on by the ray tube with respect to the local cross section of the tube. Therefore, by considering the angle between the two rays that define the tube as $d\theta_0$ and the initial (or reference) angle as θ_0 we can express the power at any range as:

$$P(r) = I(r) \cdot 2\pi r \cdot dL = I(r) \cdot 2\pi r \cdot \sin(\theta) \cdot dr \tag{3.2.1}$$

And the reference power as:

$$P_0 = I_0 \cdot 2\pi {r_0}^2 \cdot \cos(\theta_0) \cdot d\theta_0 \tag{3.2.2}$$

Since power within the tube remains constant (conservation of energy), in order to express Transmission Loss we write:

$$P(r) = P_0 \Rightarrow \frac{I(r)}{I_0} = \frac{{r_0}^2}{r} \cdot \frac{\cos(\theta_0)}{\sin(\theta)} \cdot \frac{\Delta\theta_0}{\Delta x} \tag{3.2.3}$$

$$TL(r) = -10log\left(\frac{I(r)}{I_0}\right) \tag{3.2.4}$$

There are some major problems with this scheme with the most obvious one being when the angle between the two rays θ (or L) approaches zero. At these points geometrical acoustics fail to compute the appropriate pressure field.

The regions where geometrical acoustics doesn't hold are called caustics and are formed when the refractive properties of the ocean environment focus a number of adjacent rays into close proximity. Also consequence of this effect is the forming of regions where rays are refracted out of, creating very quiet zones or *perfect shadows*.

3.3 The Eikonal Equation

In the framework of Ray Theory, the solution of the Helmholtz equation for $p(\boldsymbol{r})$ is assumed to be the product of a pressure amplitude function $A = A(\boldsymbol{r})$ and a phase function $\tau = \tau(\boldsymbol{r})$ which is referred to as "eikonal" from the Greek word for image. The solution should look like this:

$$p(\boldsymbol{r}) \sim A(\boldsymbol{r})\, e^{i\omega\tau(\boldsymbol{r})} \tag{3.3.1}$$

By substituting into the Helmholtz equation $(2.1.2)$, we calculate the derivatives which produce imaginary and real terms. Ignoring the source term, and separating real from imaginary, we get two equations:

$$\frac{1}{A}\nabla^2 A - \omega^2[\nabla\tau]^2 + k^2 = 0 \tag{3.3.2}$$

$$2[\nabla A \cdot \nabla\tau] + A\nabla^2\tau = 0 \tag{3.3.3}$$

Equation $(3.3.2)$ contains the real terms and defines the geometry of the rays. Equation $(3.3.3)$ contains the imaginary terms and determines the wave amplitudes and it is known as the transport equation. The separation of functions is performed under the assumption that the amplitude varies more slowly with position than does the phase. Assuming that the change in sound speed is small over one wavelength, we perform the approximation:

$$\frac{1}{A}\nabla^2 A \ll k^2 \tag{3.3.4}$$

This is inherently a high frequency approximation (amplitude change is small compared to the wavelength) and the equation $(3.3.2)$ now reduces to:

$$\omega^2[\nabla\tau]^2 = k^2 \Rightarrow \tag{3.3.5}$$

$$\Rightarrow [\nabla\tau(\boldsymbol{r})]^2 = \frac{1}{c(\boldsymbol{r})^2} \tag{3.3.6}$$

$(3.3.6)$ is referred to as the eikonal equation.

The rays are normal to surfaces of constant phase τ and the geometry of these surfaces is defined by the sound speed profile. This means that we can define a new coordinate system with components that are tangent and normal to the rays (ray centered). Since $\nabla\tau$ is tangent to the rays, we can define the ray trajectory as:

$$\frac{d\boldsymbol{r}(x,y)}{ds} = c\nabla\tau(x,y) \tag{3.3.7}$$

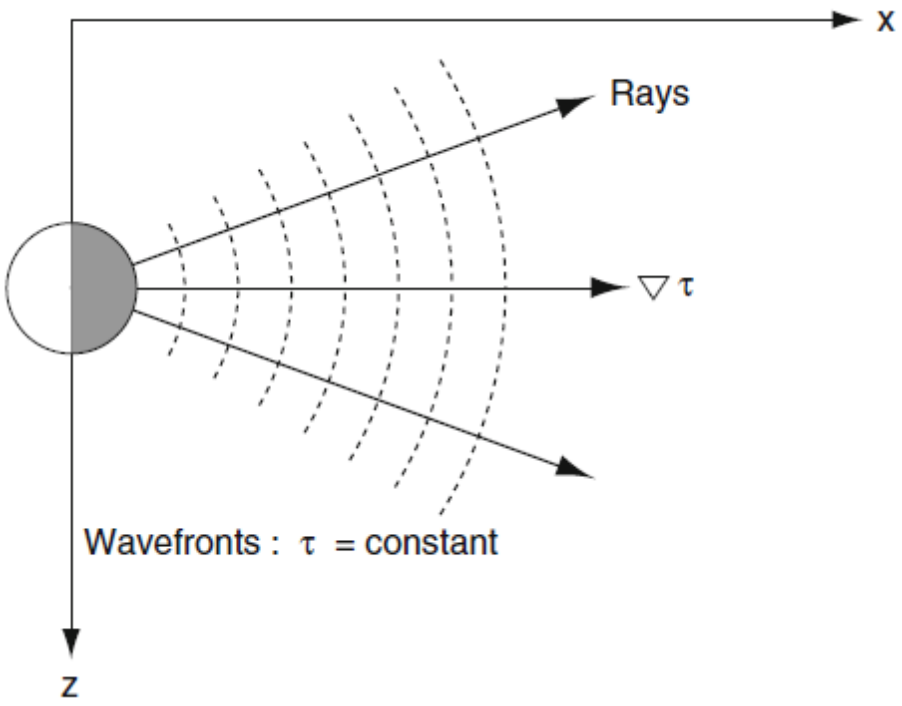

Figure 3-4

We expand the vector equation $(3.3.7)$ so that to relate $\frac{\partial x}{\partial s}$ and $\frac{\partial y}{\partial s}$ with τ :

$$for\ x \overset{(3.3.7)}{\Longrightarrow} \frac{\partial x}{\partial s} = c\left(\frac{\partial \tau}{\partial x}\right) \tag{3.3.8}$$

$$for\ y \overset{(3.3.7)}{\Longrightarrow} \frac{\partial y}{\partial s} = c\left(\frac{\partial \tau}{\partial y}\right) \tag{3.3.9}$$

We manipulate expression $(3.3.7)$ in order to eliminate the unknown function τ and end up with an expression that relates the ray centered coordinate systems with the Cartesian coordinates and the speed of sound. This technique, of reducing a second order nonlinear PDE $(3.3.6)$ to a system of first order linear equations by introducing a new, ray centered, coordinate system with $(3.3.7)$ is called *the method of characteristics*. Considering only the x component of the ray path for this derivation we begin by differentiating with ds:

$$(3.3.7)\ \frac{d\boldsymbol{r}(x,y)}{ds} = c\nabla\tau \xrightarrow{for\ x\ component} \frac{dx}{ds} = c\frac{\partial \tau}{\partial x} \Rightarrow \frac{1}{c}\frac{dx}{ds} = \frac{\partial \tau}{\partial x} \Rightarrow$$

$$\overset{\frac{d}{ds}}{\Rightarrow} \frac{d}{ds}\left(\frac{1}{c}\frac{dx}{ds}\right) = \frac{d}{ds}\left(\frac{\partial \tau}{\partial x}\right) = \frac{\partial^2 \tau}{\partial x^2}\frac{\partial x}{\partial s} + \frac{\partial^2 \tau}{\partial x \partial y}\frac{\partial y}{\partial s} = c\left(\frac{\partial^2 \tau}{\partial x^2}\frac{\partial \tau}{\partial x} + \frac{\partial^2 \tau}{\partial x \partial y}\frac{\partial \tau}{\partial y}\right) = \frac{c}{2}\frac{\partial}{\partial x}\left[\left(\frac{\partial \tau}{\partial x}\right)^2 + \left(\frac{\partial \tau}{\partial y}\right)^2\right] =$$

$$= \frac{c}{2}\frac{\partial}{\partial x}[\nabla\tau]^2 = \frac{c}{2}\frac{\partial}{\partial x}\left(\frac{1}{c^2(\boldsymbol{r})}\right) = -\frac{1}{c^2}\frac{\partial c}{\partial x}$$

Generalizing for both coordinates we can write the above in the compact vector equation form for $\boldsymbol{r}[\, r(s), z(s)\,]$:

$$\frac{d}{ds}\left(\frac{1}{c(r,z)}\frac{d\boldsymbol{r}}{ds}\right) = -\frac{1}{c^2(r,z)}\nabla \mathrm{c}(\mathrm{r},\mathrm{z}) \tag{3.3.10}$$

We obtain the standard ray equations in cylindrical coordinates (r, z) as a system of linear, first order, partial differential equations using the auxiliary variables $\xi(s)$ and $\zeta(s)$:

$$\frac{dr}{ds} = c\xi(s) \quad (3.3.11), \qquad \frac{d\xi}{ds} = -\frac{1}{c^2}\frac{\partial c}{\partial r} \quad (3.3.12)$$

$$\frac{dz}{ds} = c\zeta(s) \quad (3.3.13), \qquad \frac{d\zeta}{ds} = -\frac{1}{c^2}\frac{\partial c}{\partial z} \quad (3.3.14)$$

The tangent and the normal vectors, parameterized by arc length, can be expressed as:

$$\boldsymbol{t}_{ray} = c[\xi(s), \zeta(s)] \quad (3.3.15), \qquad \boldsymbol{n}_{ray} = c[-\zeta(s), \xi(s)] \quad (3.3.16)$$

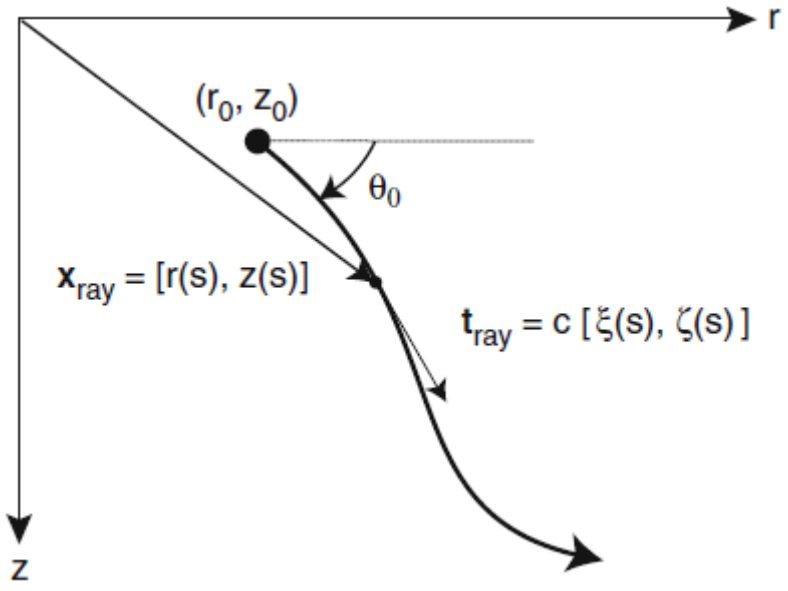

Figure 3-5

With the initial angle θ_0 being measured from the horizontal (positive values downwards, negative above), the initial conditions for launching the rays at $s = 0$ are:

$$r = r_{source}, \qquad \xi = \frac{\cos(\theta_0)}{c(0)} \tag{3.3.17}$$

$$z = z_{source}, \qquad \zeta = \frac{\sin(\theta_0)}{c(0)} \tag{3.3.18}$$

To no surprise, the initial conditions for the auxiliary variables are same with the constant we obtained through Snell's law at the previous section. These are the constants that describe the characteristics. These curves are solutions to the wave equation and in our context perfectly coincide with our description of rays.

The phase is obtained by solving the eikonal equation in the coordinate system of the rays:

$$\overset{(3)}{\Rightarrow} (\nabla\tau)\cdot(\nabla\tau) = \frac{1}{c(s)^2} \Rightarrow \ \nabla\tau \cdot \frac{1}{c}\frac{d\boldsymbol{r}}{ds} = \frac{1}{c^2} \ \Rightarrow \ \frac{d\tau}{ds} = \frac{1}{c} \ \Rightarrow$$

$$\Rightarrow \tau(s) = \tau(0) + \int_0^s \frac{1}{c(s')} ds' \tag{3.3.19}$$

The integral represents the *travel time* of the ray.

3.4 The problem of Caustics in the Transport Equation

Now, by manipulating the transport equation we'll get an expression for the amplitude of the rays. The solution is based on the observation that equation $(3.3.3)$ can be written in the form:

$$\overset{(3.3.3)}{\Longrightarrow} 2[\nabla A \cdot \nabla\tau] + A\nabla^2\tau = 0 \ \Rightarrow \nabla\cdot(A^2\nabla\tau) = 0 \tag{3.4.1}$$

Assuming constant density and by invoking the principle of conservation of energy flux of a field at a closed surface:

$$\int_S (A^2\nabla\tau)\cdot\boldsymbol{n}\, dS = 0 \tag{3.4.2}$$

We can see that the dot product of the gradient of the phase with the normal vector, $\boldsymbol{n} = \frac{d\boldsymbol{r}}{ds}$ is expressed in the above calculation of the phase:

$$\nabla\tau \cdot \frac{d\boldsymbol{r}}{ds} = \frac{1}{c} \tag{3.4.3}$$

Therefore, we obtain the following energy conservation law:

$$\int_S^{initial} \frac{A^2}{c}\, dS = \int_S^{final} \frac{A^2}{c}\, dS \tag{3.4.4}$$

In the two dimensional case, the initial surface and the final surface are the endcaps of a ray tube and the computation of the pressure amplitude follows the geometrical law for spherical spreading:

$$A_f = \left(\frac{c_f d\sigma_i}{c_i d\sigma_f}\right)^{1/2} A_i \tag{3.4.5}$$

Where $A_f = A(x_f, y_f)$, $A_i = A(x_i, y_i)$ the final and initial amplitudes and: $c_f = c(x_f, y_f)$, $c_i(x_i, y_i)$ are the sound speeds and $d\sigma_f$, $d\sigma_i$ the cross sections. As $d\sigma_f$ approaches zero A_f approaches infinity, effectively creating infinite pressure. This is the problem of caustics which has been already discussed.

3.5 Solution of the Transport Equation

The transport equation, was left as an expression $(3.4.24)$ of amplitudes and cross sections of the tube, which instead of final and initial, we express now, as an amplitude at the start of the ray $s = 0$ and an amplitude at a ray point s.

$$A(s) = \left(\frac{c_f d\sigma_0}{c_i d\sigma_s}\right)^{1/2} A(0)$$

Examining Figure 3-3 we derive that the cross section $d\sigma(s)$ of the two dimensional ray tube is:

$$d\sigma_s = -s^2 cos\theta_0 \tag{3.5.1}$$

In order to proceed to the calculation of the Amplitude for $s = 0$ we need to remind that the solution for a point source in three dimensions is:

$$p(s) = \frac{1}{4\pi s} e^{i\omega s/c} \tag{3.5.2}$$

Therefore:

$$A(s) = \frac{1}{4\pi s} \tag{3.5.3}$$

Which approaches infinity when $s \to 0$. But we can reach a bounded quantity if we consider:

$$\lim_{s\to 0} A(s)\,|d\sigma(s)|^{1/2} = \frac{1}{4\pi}\,|cos\theta_0|^{1/2} \tag{3.5.4}$$

Finally the amplitude at a point s is given by:

$$A(s) = \frac{1}{4\pi}\left|\frac{c(s)cos\theta_0}{c(0)d\sigma(s)}\right|^{1/2} \tag{3.5.5}$$

4 Gaussian Beams Theory

In the previous section we derived the standard ray equations from the eikonal and this description of ray paths is going provide the backbone for the Gaussian Beams.

We've seen two methods of tracing acoustic rays as they propagate through the underwater environment and in both methods we encountered the existence of caustics in ray focal points. The consequence of rays focusing on certain areas is that some other areas remain devoid of rays, effectively creating perfect shadows. In comparison to standard ray tracing, the method of Gaussian Beams is free of these artifacts and the pressure calculation does not need to suffer from eigenray computation (that is to find out how many rays hit a receiver).

The standard ray equations we derived in the previous section are used to calculate the ray path and form the center of the beam. The ray centered coordinates are: (s, n) with s being tangent and n normal to the ray. The initial step in constructing a Gaussian Beam is to divide the pressure function, in ray centered coordinates, in three parts. First part controls amplitude, second part is an envelope function that imposes the Gaussian and third part is phase:

$$p_{beam}(s,n) = A_{beam}(s)\, \Phi(s,n)\, e^{-i\omega\tau(s)} \tag{4.1.1}$$

4.1 Complex Source Point Approach

Before the citation of the appropriate pressure equation for the Gaussian Beams, let's search for an expected form of $\Phi(\boldsymbol{r})$. The exact solution, for a point source in free space, with $\boldsymbol{r} = (x, z)$ and r_0 the coordinates of the source, is:

$$p(\boldsymbol{r}) = \frac{e^{ik|\boldsymbol{r}-r_0|}}{|\boldsymbol{r}-r_0|}, \qquad k = \frac{\omega}{c} \tag{4.1.2}$$

We pick $r_0 = (ia, 0)$, so that the r coordinate has been offset to the complex plane. This produces a beam centered on the x-axis and the denominator now reads:

$$|\boldsymbol{r}-r_0| = \sqrt{(x-ia)^2 + z^2} \tag{4.1.3}$$

The square root can be approximated using the Taylor series expansion as:

$$\sqrt{(x-ia)^2+z^2} \approx (x-ia) + \frac{z^2}{2(x-ia)} - \cdots \tag{4.1.4}$$

Assuming solutions close to the axis of the beam ($z \ll x$) we can neglect the z^2 term in the denominator. Therefore, the approximation for pressure reads:

$$p(\boldsymbol{r}) \approx \frac{e^{ka}e^{ikx}}{x-ia} \cdot exp\left\{ik\frac{z^2}{2(x-ia)}\right\} = \tilde{A}(x) \cdot exp\left\{ik\frac{(x+ia)}{2(x^2+a^2)}z^2\right\} =$$

$$= \tilde{A}(x) \cdot e^{\frac{ik}{2}\left[\frac{x}{x^2+a^2}\right]z^2} \cdot e^{-\left[\frac{ka}{2(x^2+a^2)}\right]z^2} \tag{4.1.5}$$

We recognize the terms $K(x)$ as curvature of the phase fronts and $W(x)$ as the width of the beam:

$$K(x) = \frac{x}{x^2 + a^2} \quad (4.1.6)\,, \quad W(x) = \sqrt{\frac{2(x^2 + a^2)}{ka}} \quad (4.1.7)$$

The half width, or radius of the beam, is defined as the distance of the center of the ray at which the beam amplitude is $1/e$ of its maximum value. There is a limit imposed to the minimum width of the beam so to avoid caustics. An empirically derived focal limit is $\pi \cdot \lambda$.

Finally, rewriting $p(\boldsymbol{r})$ as:

$$p(\boldsymbol{r}) \approx \tilde{A}(x) \cdot e^{\frac{ik}{2} K(x)\, z^2} \cdot e^{-\left(\frac{z}{W(x)}\right)^2} \quad (4.1.8)$$

We expect $\Phi(\boldsymbol{r})$ to be an exponent containing the curvature and beamwidth terms:

$$\Phi(s, n) \cong e^{\frac{ik}{2} K(x)\, z^2} e^{-\left(\frac{z}{W(x)}\right)^2} \quad (4.1.9)$$

4.2 Dynamical Equations

The implementation of Gaussian Beams invokes a set of ray centered differential equations that calculate a beam width $q(s)$ and a beam curvature $p(s)$ along the ray:

$$\frac{dq}{ds} = c(s)p(s) \quad (4.2.1), \qquad \frac{dp}{ds} = -\frac{c_{nn}}{c^2(s)} q(s) \quad (4.2.2)$$

For the derivation of the above relations and the beam pressure equation, the reader is referred to Cerveny et al (1982) and also Porter and Bucker (1987).

c_{nn} is the second derivative of the sound speed along the normal of the ray and can be calculated with direct double differentiation invoking the use of the normal vector to the ray (see section 4.) and expressed in terms of auxiliary variables ξ and ζ:

$$c_n(r, z) = \nabla c(r, z) \cdot \boldsymbol{n}$$

$$c_{nn}(r, z) = \nabla c_n(r, z) \cdot \boldsymbol{n} = c^2 \left(\frac{\partial^2 c}{\partial r^2} \zeta^2 - 2 \frac{\partial^2 c}{\partial r \partial z} \zeta \xi + \frac{\partial^2 c}{\partial z^2} \xi^2 \right) \quad (4.2.3)$$

We can manage a more accurate description of the beam in terms of $q(s)$ and $p(s)$ defined as:

$$p_{beam}(s, n) = A \sqrt{\frac{c(s)}{r q(s)}} \cdot e^{-i\omega \frac{n^2}{2} \frac{p(s)}{q(s)}}\, e^{-i\omega \tau(s)} \quad (4.2.4)$$

The curvature K and beam width W we derived with the complex point source method relate with the quantities $q(s)$ and $p(s)$ through these equations:

$$W(s) = \sqrt{\frac{-2}{\omega \mathrm{Im}\left[\frac{p(s)}{q(s)}\right]}} \quad (4.2.5), \qquad K(s) = -c(s)\mathrm{Re}\left[\frac{p(s)}{q(s)}\right] \quad (4.2.6)$$

4.3 Initial Conditions for $q(s)$ and $p(s)$

In order to start computing $q(s)$ and $p(s)$ in terms of ray steps, we need to specify initial conditions. The amplitude of the beam is also specified at the initial state by the constant A and then it evolves with the beam. The beam, starts from the point source as flat and travels the waveguide until the specified end.

To set the initial curvature as flat we simply impose:

$$p(0) = 1 \quad (4.3.1)$$

The initial beamwidth should be chosen such as that the beams diverge rapidly and become large compared to the water depth in the farfield but are not large compared to the water depth when starting from the source. When the beams reach the end of the waveguide, which is in the farfield, we want them to be "space filling", meaning that they have to have a reasonable coverage. Porter chooses this so that the influence of a beam to be reduced by $1/e$ at the location of its two neighboring beams. This is a little trickier.

Let's assume initially that:

$$q(0) = i\varepsilon \quad (4.3.2)$$

By solving the equations we get:

$$\frac{p(s)}{q(s)} = \frac{c_0 s - i\varepsilon}{{c_0}^2 s^2 + \varepsilon^2} \quad (4.3.3)$$

Plugging this into $e^{-i\omega\frac{n^2}{2}\frac{p(s)}{q(s)}}$ and keeping only the expression with ε we get:

$$e^{-\omega\frac{n^2}{2}\frac{\varepsilon}{{c_0}^2 s^2 + \varepsilon^2}} \quad (4.3.4)$$

By defining the initial angular spread in which N beams are launched $[a_1, a_2]$, then each beam occupies an angle of:

$$\delta\alpha = \frac{a_2 - a_1}{N - 1} \quad (4.3.5)$$

and approximating long range as:

$$c_0 s \gg \varepsilon \quad (4.3.6)$$

and the normal distance to neighboring rays as:

$$n = s\delta a\varepsilon \tag{4.3.7}$$

Then, in order to be consistent with the definition of "space filling":

$$e^{-\omega \frac{s^2\delta\alpha^2}{2}\frac{\varepsilon}{{c_0}^2 s^2}} = e^{-\omega \frac{\delta\alpha^2}{2}\frac{\varepsilon}{{c_0}^2}} = {}^1\!/_e \Rightarrow \omega \frac{\delta\alpha^2}{2}\frac{\varepsilon}{{c_0}^2} = 1 \Rightarrow$$

$$\Rightarrow \varepsilon = \frac{2{c_0}^2}{\omega\delta\alpha^2} \tag{4.3.8}$$

Therefore the initial condition for $q(s)$ is:

$$q(0) = i\frac{2{c_0}^2}{\omega\delta\alpha^2} \tag{4.3.9}$$

4.4 Starting Amplitude

Final step is to calculate the arbitrary constant A. This is done by matching the exact solution of the pressure for a point source in a homogeneous medium in three dimensions:

$$p(R) = \frac{e^{-i\omega\frac{R}{c_0}}}{R} \tag{4.4.1}$$

With the high frequency asymptotic approximation using the saddle point method of the integral over all beam launch angles of the beam pressure expression. This integral represents the total pressure field:

$$p(a_0) = \int A(a)\sqrt{\frac{c(s)}{rq(s)}}\cdot e^{-i\omega\frac{n^2}{2}\frac{p(s)}{q(s)}}\cdot e^{-i\omega\tau(s)}da \;\approx\; A(a_0)c_0\sqrt{\frac{2\pi}{q(0)\omega\,\boldsymbol{r}R}}\cdot e^{-i\omega\frac{R}{c_0}}\cdot e^{-i\frac{\pi}{4}}$$

(4.4.2)

In the above expression a_0 is the angle to the receiver, R the slant range to the receiver and $\boldsymbol{r}$ the cylindrical coordinates to the receiver which can be written as:

$$\boldsymbol{r} = Rcos(a_0)$$

Finally we are able to extract $A(a)$ as:

$$A(a) = \frac{1}{c_0}e^{i\frac{\pi}{4}}\sqrt{\frac{q(0)\omega\cos(a)}{2\pi}} = \frac{e^{i\frac{\pi}{2}}}{\delta\alpha}\sqrt{\frac{\cos(a)}{\pi}} \tag{4.4.3}$$

4.5 Gaussian Beams

The final expression for the pressure of a Gaussian Beam is:

$$p_{beam}(s,n) = \sqrt{\frac{\cos(\alpha)}{\pi}}\; e^{\frac{i\pi}{2}} \sqrt{\frac{c(s)}{rq(s)}}\; e^{-i\omega\frac{n^2}{2}\frac{p(s)}{q(s)}}\; e^{-i\omega\tau(s)} \tag{4.5.1}$$

Therefore, the total pressure field of the problem at hand, is represented by a source that launches N beams over an angular opening $[a_1, a_2]$ and imposed the condition to "fill" the waveguide:

$$P(a) = \sum^{N} \sqrt{\frac{\cos(\alpha)}{\pi}}\; e^{\frac{i\pi}{2}} \sqrt{\frac{c(s)}{rq(s)}}\; e^{-i\omega\frac{n^2}{2}\frac{p(s)}{q(s)}}\; e^{-i\omega\tau(s)} \tag{4.5.2}$$

5 Pressure Field Calculation

The final pressure field is calculated by introducing a grid of receivers, which is usually rectangular. With Gaussian Beams the pressure field is a summation over the contribution of every beam at the given receiver which implies finding the distance of the Beam to the receiver and the pressure (or intensity) at that distance. At each ray stepping, the distance between the initial and the final ray position includes a number of receivers, laying in columns, at which we wish to calculate the pressure. For each receiver column the summation is done sequentially from the surface all the way down to the bottom.

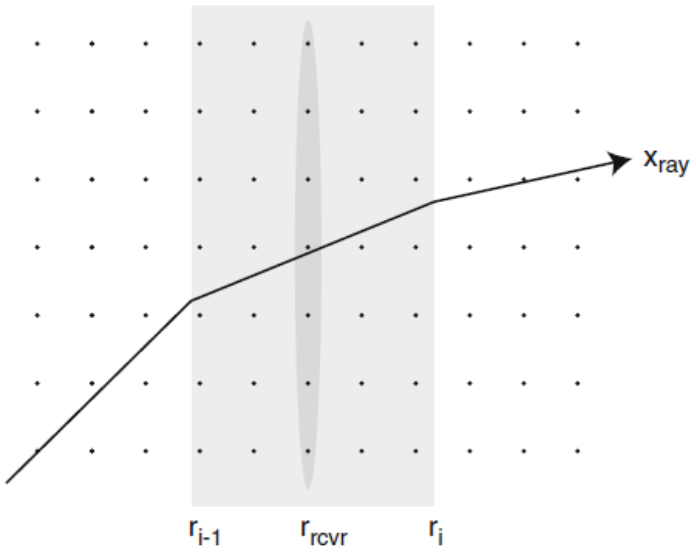

Figure 5-1 Ray stepping into a receiver grid

5.1 Finding the Receiver Distance

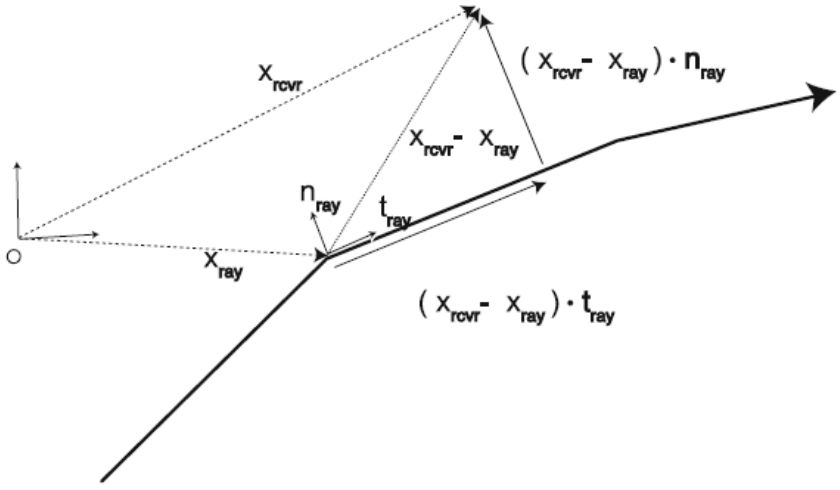

Figure 5-2 Ray - Receiver distance

Each receiver location in Cartesian coordinates (r, z) must be mapped in ray-centered coordinates (s, n). The ray centered coordinates for each receiver are derived from vector analysis:

$$s = (\boldsymbol{x}_{rcvr} - \boldsymbol{x}_{ray}) \cdot \boldsymbol{t}_{ray} \tag{5.1.1}$$

$$n = \left|(\boldsymbol{x}_{rcvr} - \boldsymbol{x}_{ray}) \cdot \boldsymbol{n}_{ray}\right| \tag{5.1.2}$$

Where: $\boldsymbol{x}_{ray} = (\boldsymbol{r}_{ray}, \boldsymbol{z}_{ray})$.

5.2 Interpolating Between Ray Steps

Any required value for the beam, like $\tau(s), q(s), p(s)$, that lies between initial and final ray steps, can be calculated with linear interpolation between the values at the endpoints. For instance, $q(s)$, which governs the beam amplitude, is computed as:

$$q = q_{i-1} + a(q_i - q_{i-1}) \tag{5.2.1}$$

Where a is the proportional distance along a ray step:

$$a = \frac{s}{|r_i - r_{i-1}|} \tag{5.2.2}$$

5.3 Pressure Summation

After calculating the distance of a receiver from the central ray of the beam, we can use the s and n receiver coordinates to calculate the pressure at that point. The different approaches of handling phase in pressure summation are briefly presented below assuming that N beamwidths reach the receiver point. This is the most computational intensive aspect of the algorithm so some restrictions can be imposed for contributing beams (e.g. five beam widths distance).

5.3.1 Coherent Addition

Adding the pressure intensity of each beam hitting a single receiver coherently is the proper way to represent the field. Very simply:

$$P_{Coh} = \sum_{j=1}^{N} p_{beam}^{j}(s_{rcvr}, n_{rcvr}) \tag{5.3.1}$$

5.3.2 Incoherent Addition

Sometimes the phasing details of the problem may be unimportant to the user or may be a factor that in real applications is essentially incalculable. To sum incoherently:

$$P_{Inc} = \left[\sum_{j=1}^{N} \left| p_{beam}^{j}(s_{rcvr}, n_{rcvr}) \right|^2 \right]^{1/2} \tag{5.3.2}$$

5.3.3 Semicoherent Addition

This is an intermediate solution that aims to retain the gross phasing patterns and features while smoothing out the bad features of rays. The semicoherent calculation is defined by:

$$P_{SemInc} = \left[\sum_{j=1}^{N} S(\theta_0) \left| p_{beam}^{j}(s_{rcvr}, n_{rcvr}) \right|^2 \right]^{1/2} \tag{5.3.3}$$

$S(\theta_0)$ is weighting the amplitude of the ray as a function of its take off angle.

This particular weighting function reconstructs the Lloyd mirror pattern in the nearfield and it's used by BELLHOP:

$$S(\theta_0) = 2\sin\left(\frac{\omega z_0 \sin(\theta_0)}{c_0}\right) \tag{5.3.4}$$

6 Tracing Beams with Direct Integration

We've seen that tracing an individual beam is a problem of integrating the set of coupled nonlinear ordinary differential equations presented on the previous sections. This is done with the scheme of *second order Runge-Kutta method*:

$$y_{i+1/2} = y_i + \frac{h}{2}\boldsymbol{f}(x_i, y_i), \tag{6.1}$$

$$y_{i+1} = y_i + h\boldsymbol{f}(x_{i+1/2}, y_{i+1/2}) \tag{6.2}$$

High efficiency can be achieved by implementing a varying step size h.

7 Bottom Interaction

7.1 Bottom Loss

To address the problem of acoustic waves that fall at an interface separating two fluid media (no shear waves) with densities ρ_1 and ρ_2 and sound speeds c_1 and c_2 , we approximate the incident, reflected and transmitted wave as plane waves. At the interface we apply the boundary conditions below, expressing continuity of pressure and vertical component of the particle velocity:

$$p_1 = p_2 \,, \tag{7.1.1}$$

$$\frac{1}{\rho_1}\frac{\partial p_1}{\partial z} = \frac{1}{p_2}\frac{\partial p_2}{\partial z} \tag{7.1.2}$$

p_1 is the acoustic pressure at the water and p_2 is the acoustic pressure at the sea-bed, just above and below the interface correspondingly. The acoustic pressure at the water is the sum of the incident $p_i$and reflected pressure p_r. Applying the appropriate solutions of the acoustic wave equation for plane waves and expressing the reflection coefficient as the ratio of the reflected to the incident pressure, we obtain the following expression for the reflection coefficient:

$$R = \frac{\rho_2 c_2/\sin(\theta_2) - \rho_1 c_1/\sin(\theta_1)}{\rho_2 c_2/\sin(\theta_2) + \rho_1 c_1/\sin(\theta_1)} \tag{7.1.3}$$

where $\theta_1$is the grazing angle of the incident wave and θ_2 is the angle of the transmitted wave, connected through Snell's law.

The reflection coefficient is a measure of the acoustic intensity that "returns" to the water column, as in the case of water-bottom interaction there is potentially a loss of energy in the sea-bed.

As the reflec*Bottom Loss* is considered an attenuation component of Transmission Loss and is defined as:

$$BL = -10\log|R|^2 \tag{7.1.4}$$

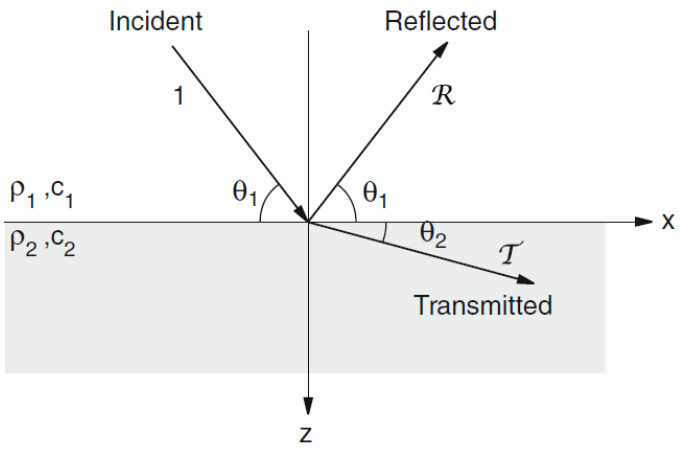

Figure 7-1 Ray - Bottom interaction

For multilayered bottoms or bottoms that support shear waves the reflection coefficient becomes a complex number and the interested reader can refer to Jensen et al. (2011).

7.2 Correcting the Ray Step

In order for the ray to land exactly on the boundary, the implementation of a "*test step*", $\tilde{h}$ is in order. If the test step crosses a top or bottom boundary then the real step must be reduced accordingly. If D is the depth of the problem and we are defining the cross in terms of depth position z_i of the ray, then:

$$\tilde{h} = \frac{|D - z_i|}{c_i \zeta_i} \tag{7.2.1}$$

In the more general case of a range depended bottom the calculation of the reduced step is done in terms of the vectors tangent to the ray and normal to the boundary with final result:

$$\tilde{h} = \frac{\left|x_{ray} - x_{bdry}\right| \cdot \boldsymbol{n}_{bdry}}{\boldsymbol{t}_{ray} \cdot \boldsymbol{n}_{bdry}} \tag{7.2.2}$$

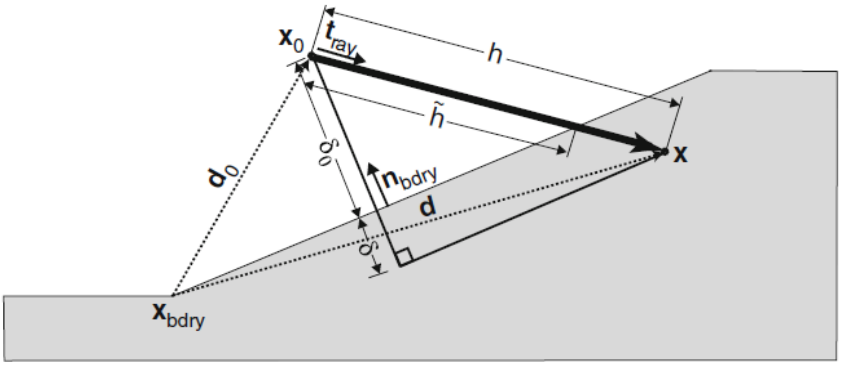

Figure 7-2 Correcting the Ray step

7.3 Updating the Ray Equations after a Bottom Reflection

A simple and most practical approach for modeling the bottom boundary is to use piecewise linear interpolation.

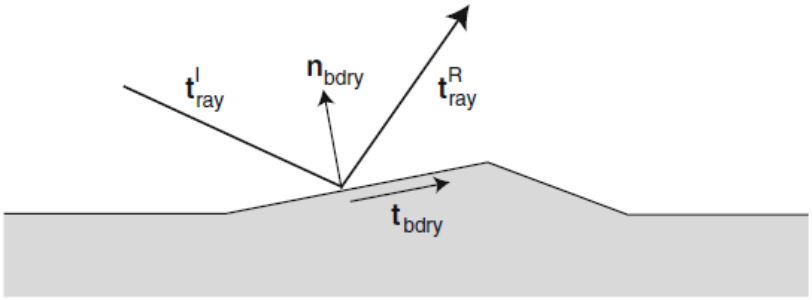

Figure 7-3 Ray reflection from piecewise linear boundary

The normals and tangents to the boundary can easily be computed by the nodal coordinates and the signs follow the convention of figure 8-3. With some simple vector analysis we can derive the reflected ray trajectory for any boundary:

$$\alpha = \left(\boldsymbol{t}^I_{ray} \cdot \boldsymbol{n}_{bdry}\right) \quad (7.3.1), \qquad \beta = \left(\boldsymbol{t}^I_{ray} \cdot \boldsymbol{t}_{bdry}\right) \quad (7.3.2)$$

$$\boldsymbol{t}_{ray}^{\boldsymbol{R}} = -\alpha \boldsymbol{n}_{bdry} + \beta \boldsymbol{n}_{bdry} \tag{7.3.3}$$

After interacting with a boundary the ray must be restarted with appropriate new conditions for the standard ray equations:

$$r^R = r^I \quad (7.3.4), \qquad \xi^R = \xi^I \quad (7.3.5)$$

$$z^R = z^I \quad (7.3.6), \qquad \zeta^R = -\zeta^I \quad (7.3.7)$$

and for the dynamical equations governing the curvature and amplitude of the beam:

$$q^R = q^I \tag{7.3.8}$$

$$p^R = p^I + q^I * N \tag{7.3.9}$$

Where:

$$N = \frac{\beta}{\alpha}(4c_n - 2\frac{\beta}{\alpha}c_s) \tag{7.3.10}$$

$$c_n = \nabla c \cdot \boldsymbol{n}_{ray} \quad (7.3.11), \qquad c_s = \nabla c \cdot \boldsymbol{t}_{ray} \quad (7.3.12)$$

Since q is amplitude we may interpret the last set of equations as that there is no change of energy on reflection but there is change in curvature. But typically there is a **Bottom Loss** associated with boundary reflections, therefore we track such losses though the usage of the amplitude function for the beam $A(s)$:

$$A^R = |R(\theta)|\, A^I \tag{7.3.13}$$

and for the updated phase:

$$\tau^R = \tau^I - arg\{R(\theta)\} \tag{7.3.14}$$

One shortcoming of this treatment is that for rays of grazing incidence there can be issues with the pressure filed.

Finally, ray trace can be terminated after an amplitude threshold or the number of boundary interactions, for further efficiency.

8 Applications with the BELLHOP program

BELLHOP was developed my Michael Porter and is a highly efficient Ray Trace program written in Fortran. It was designed to perform two dimensional ray tracing for a given sound speed profile $c(z)$ or a given sound speed field $c(r, z)$, in ocean waveguides with flat or variable absorbing boundaries. The program works with input files that provide all the information about the type of calculations, the shape of the environment and the numeric values of the parameters. Output options include ray coordinates, travel time, amplitude, eigenrays, acoustic pressure or Transmission Loss (coherent, incoherent or semi-coherent). The calculation of acoustic pressure is based on the theory of Ray Centered Gaussian Beams with the ability of some variations and uses the computational treatment mentioned in the above sections.

8.1 The Munk Profile

The Munk profile was named after Walter Heinrich Munk, an American physical oceanographer. It constitutes a standard for benchmarking acoustic software because of its characteristic SSP with a smooth acoustic channel and a large depth sea which, combined, allow the formation of caustics and therefore a good testing ground for algorithms. To the left we see the SSP plot and next to it a standard ray trace run with 51 rays of 50Hz frequency. The range independent (flat) bottom is modeled as a fluid with $c_p = 1600\,{}^{m}/_{s}$. The aperture of the source is limited to 44.6° so the source is not omnidirectional. This is done in order to not overwhelm the plot with rays. A single source has been placed at $z_{source} = 1000m$.

Notice how the focal points where caustics form for the Munk profile how they tend to fall close to the SSP minimum:

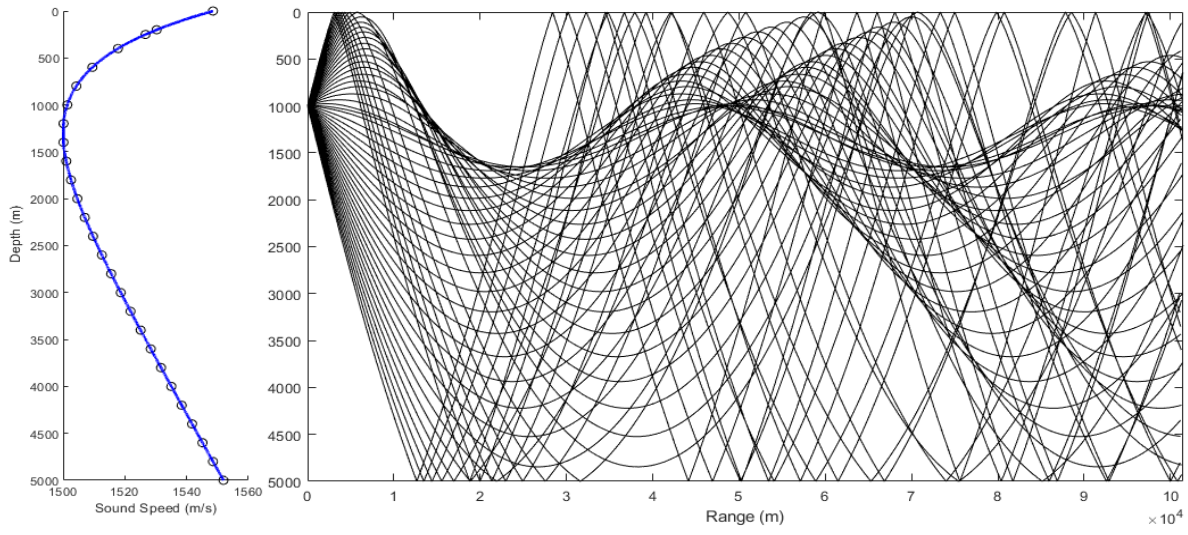

Figure 8-1.1 Munk SSP and Ray Trace

In the next two plots, the coherent Transmission Loss of an omnidirectional $(-90°, 90°)$ source is presented. It is clear that BELLHOP manages to represent acoustic pressure extremely close to the normal mode solution with KRAKEN, but with limitations in the regions where rays don't travel.

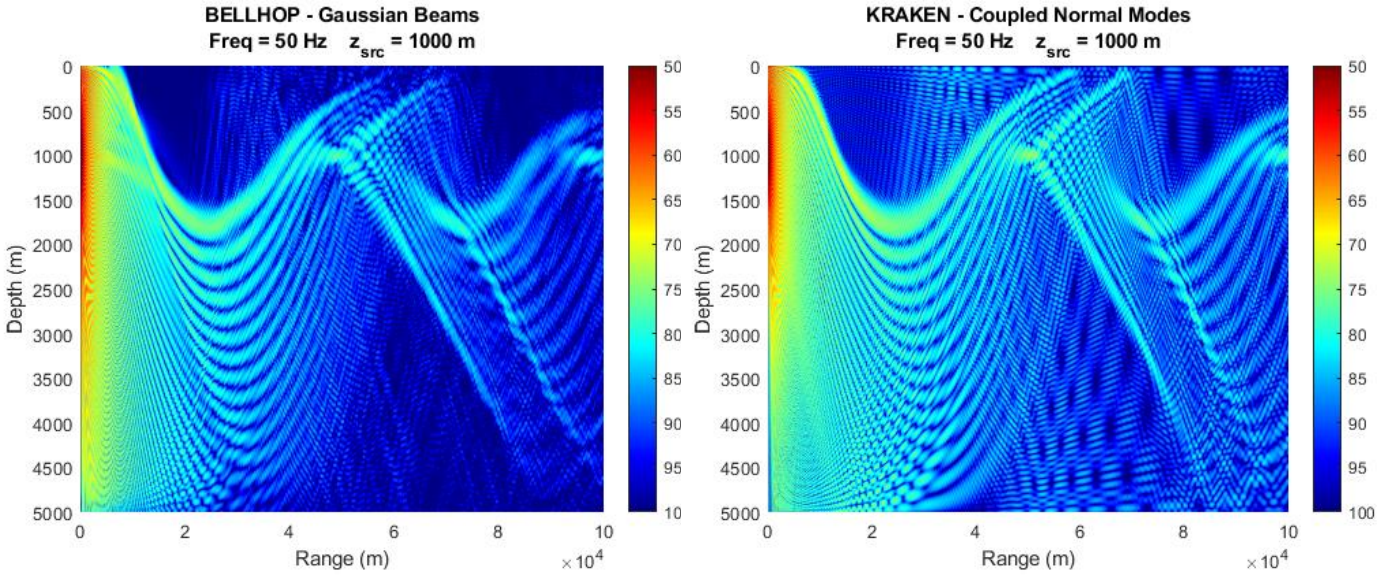

Figure 8-1.2 BELLHOP and KRAKEN for the Munk Profile

In the third plot that follows, the Transmission Loss versus range has been plotted for a fixed depth of $z_{range} = 1500m$. The almost perfect congruity of the models is clear. A slight difference can be acknowledged at the position of the first caustic at $2500m$ range, which can be contributed to the handling of such artifacts in BELLHOP as imposing minimum beam width.

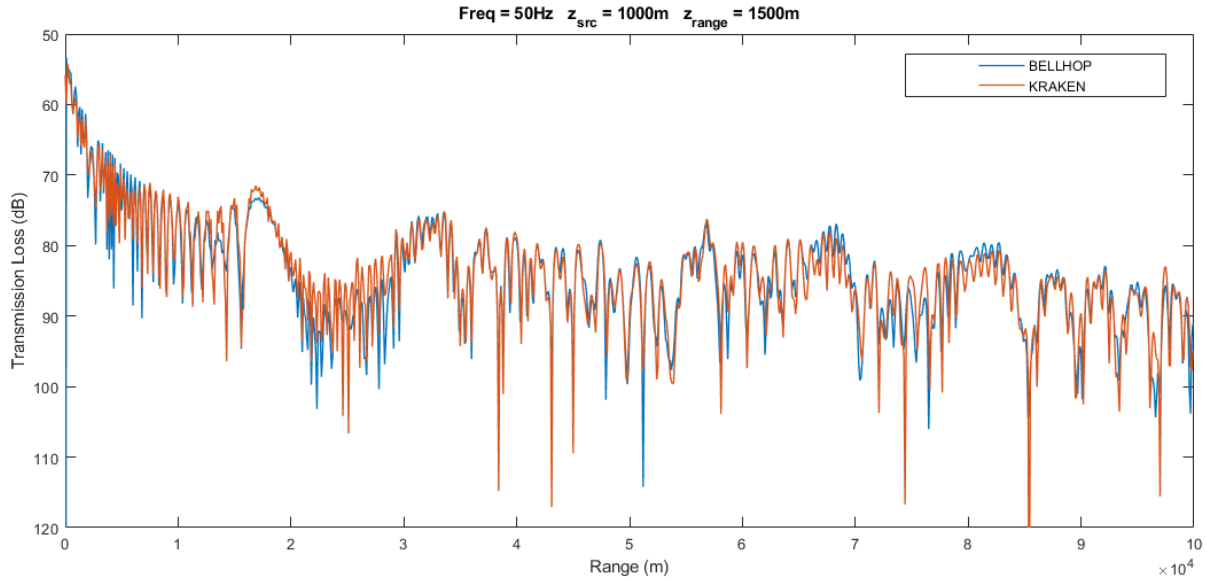

Figure 8-1.3 BELLHOP and KRAKEN fixed depth TL

Notice how BELLHOP fails at the direction of $90°$ because of the $\cos(a)$ term in the beam pressure.

8.2 Seamount & Upslope Propagation

Next case is a simple underwater mount and an extension of the mount resembling an upslope. The reasoning behind this simple example is to examine how BELLHOP treats range depended bathymetry in a controlled environment. For the Seamount example we are interested mostly in the field after the mount because of rays interacting with the seabed and then propagating. For the Upslope we are interested to see how multiple interactions with the bottom are treated. BELLHOP treats bottom interaction as an attenuated reflection but KRAKEN as the end point of normal modes and treats the bottom as an absorbing boundary by solving for continuation, which is more formal. Same as before we will plot the Transmission Loss versus range and depth and Transmission Loss versus range. To further investigate the models behavior in range depended bathymetry, two more TL vs. depth plots are added at fixed ranges of 5 and $15\ km$. We will also further extend the investigation for two frequencies at 100 and $500\ Hz$. Since the maximum depth is $D = 500m$ we have placed the source at $z_{src} = 100m$. The Seamount is a simple triangular shaped underwater hill of $250m$ height. The parameters of the bottom are: $c_p = 1650\ {}^{m}/_{s}$, density of $\rho = 1.25\ {}^{gr}/_{m^3}$ and attenuation of $0.25\ {}^{dB}/_{\lambda}$. We have used a simple SSP which defined by 3 points:

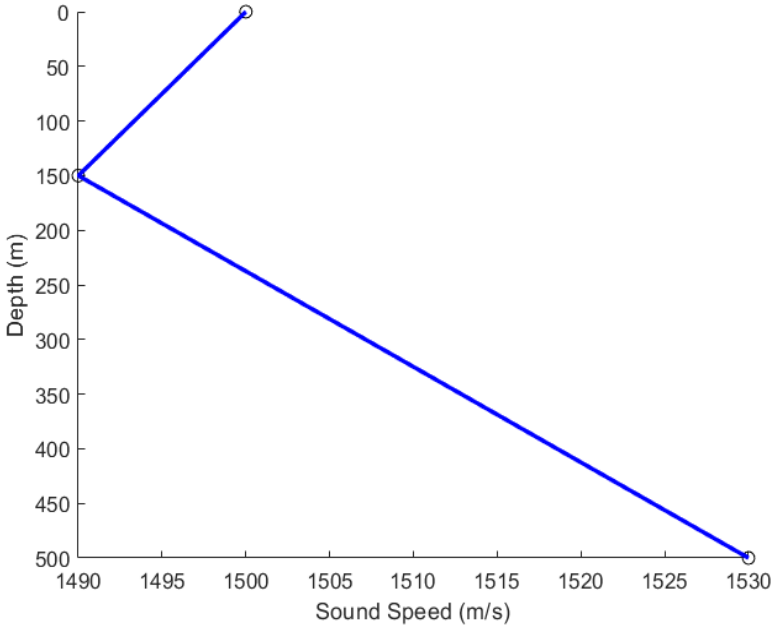

Figure 8-1 The SSP used for the Seamount and Upslope cases

In general, it seems that BELLHOP is handling the interaction of rays with the bottom with higher attenuation than the normal mode solution. This is a matter of attenuation treatment and therefore an issue that the user can resolve with better description of attenuation by providing a tabulated bottom reflection coefficient. It is also known that there is an issue in handling grazing angles in Gaussian Beams treatment (the N factor in treating boundary interaction with beams).

What we are mostly interested in benchmarking Beams versus Normal Modes, is that we get the same general structure of the coherent pressure field.

8.2.1 Seamount

First, a ray trace for the Seamount environment. The green colored paths indicate rays that interact only with the surface while the red colored manage to have zero interactions with the boundaries.

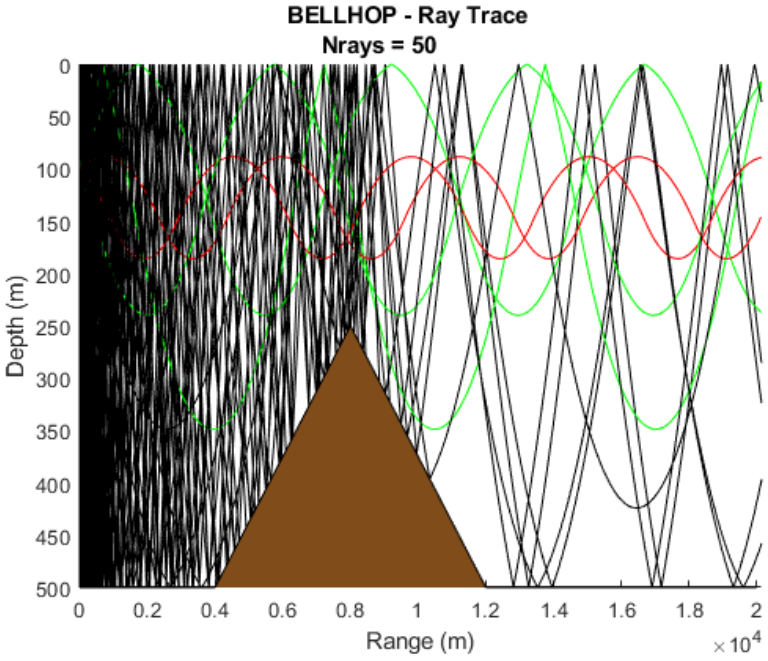

Figure 8-2 Seamount Ray Trace

Next, we trace a single Gaussian Beam (Nbeam = 26), one of the red colored ones (zero interactions). We can see the handling of focal points, and the spreading of the beamwidth.

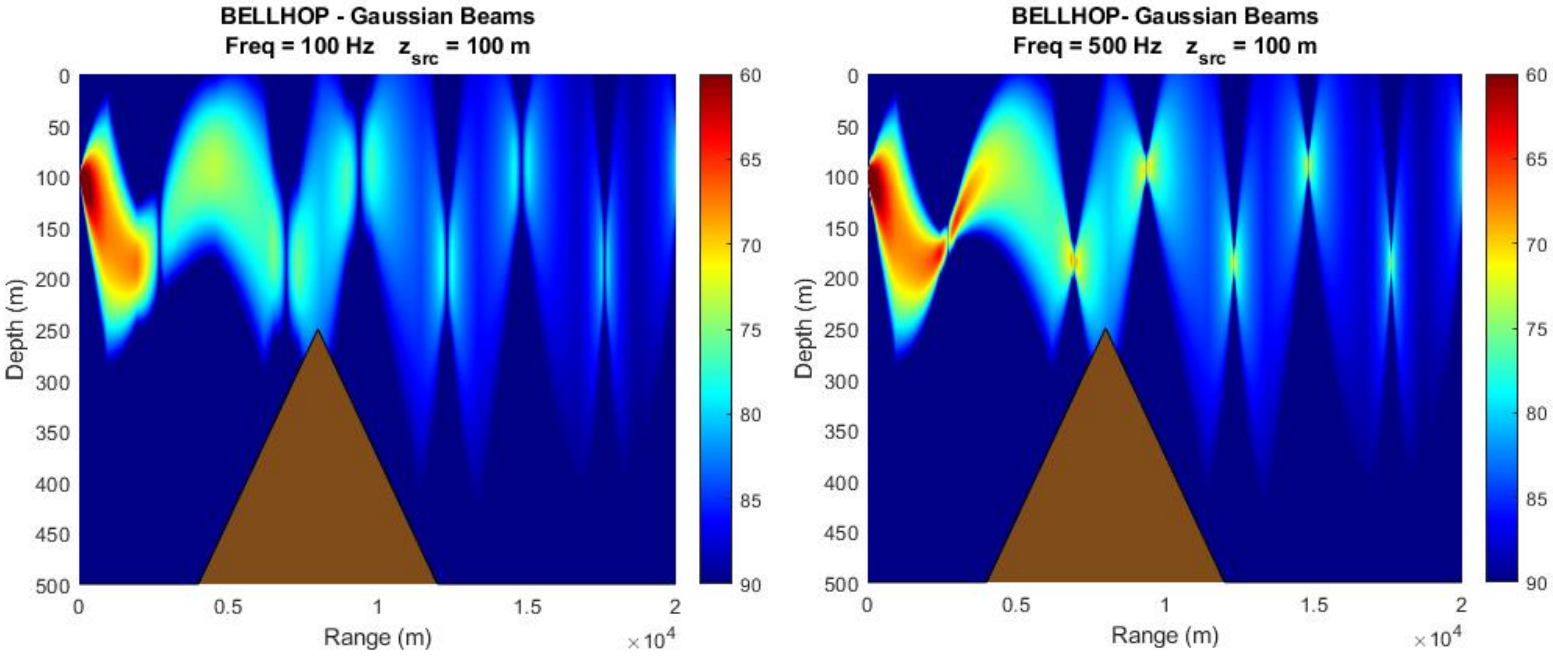

Figure 8-3 Gaussian Beam #26 of 50 at 100Hz and 500Hz

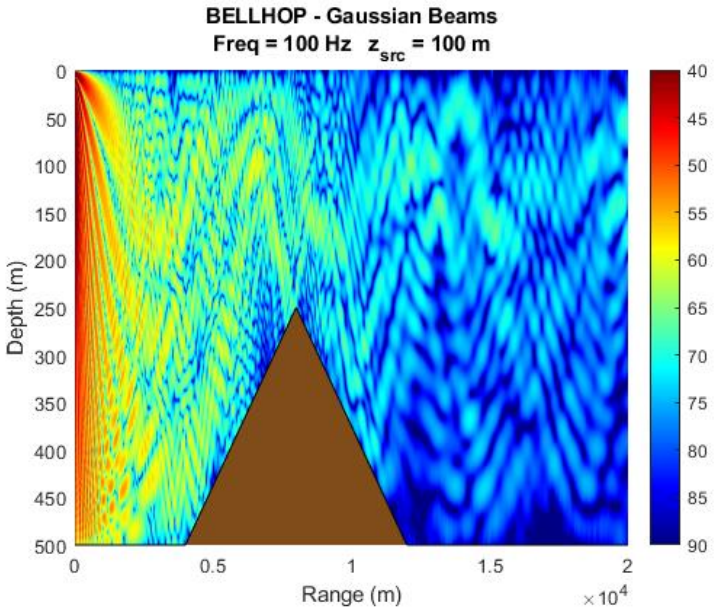

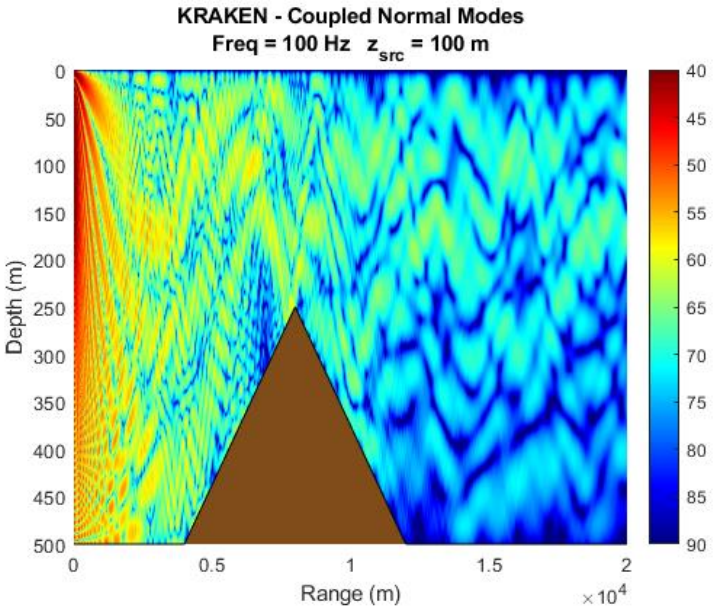

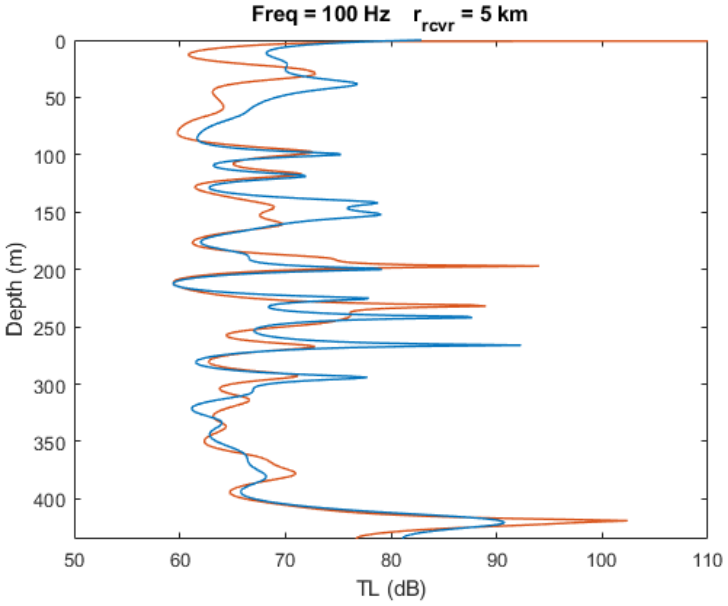

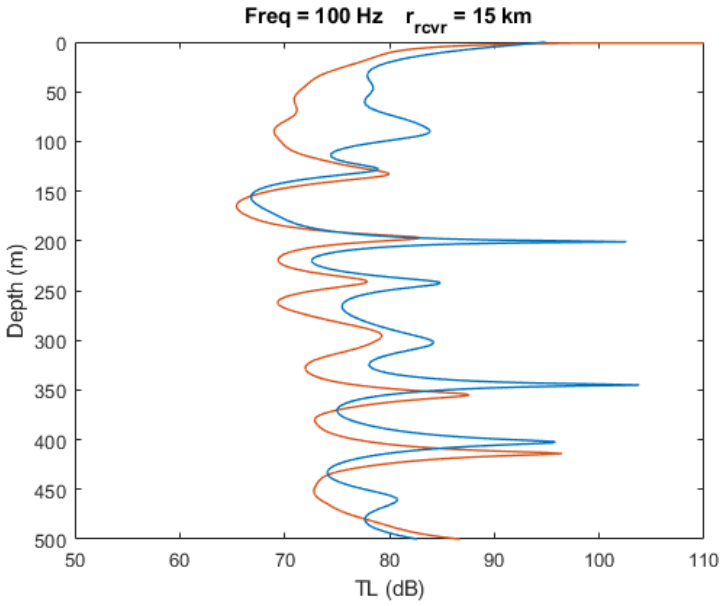

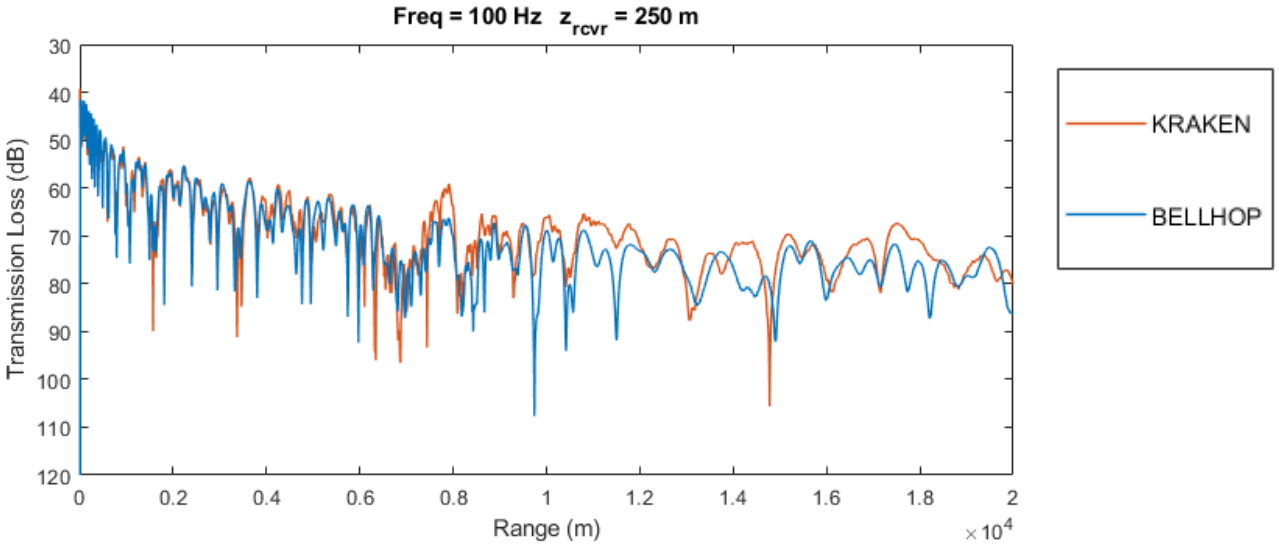

Figures 9-4, 9-5 - TL vs. Range and Depth. Figures 9-6, 9-7 - TL vs. Depth. Figure 9-8 - TL vs. Range.

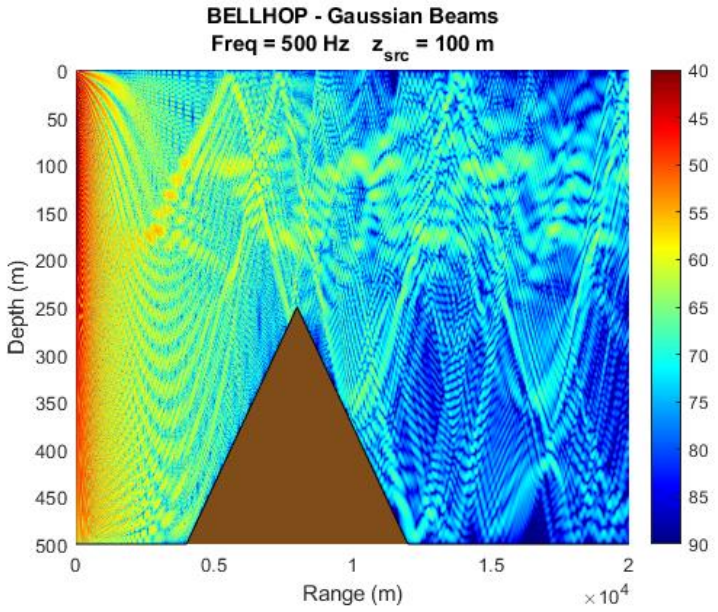

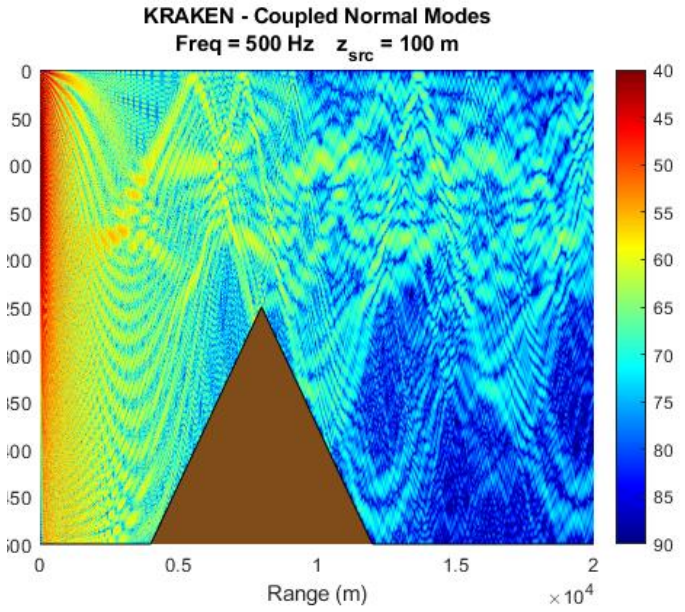

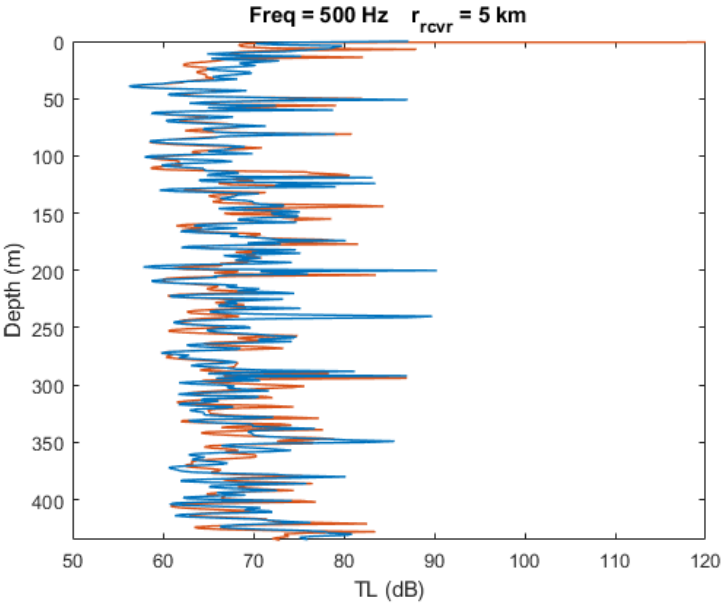

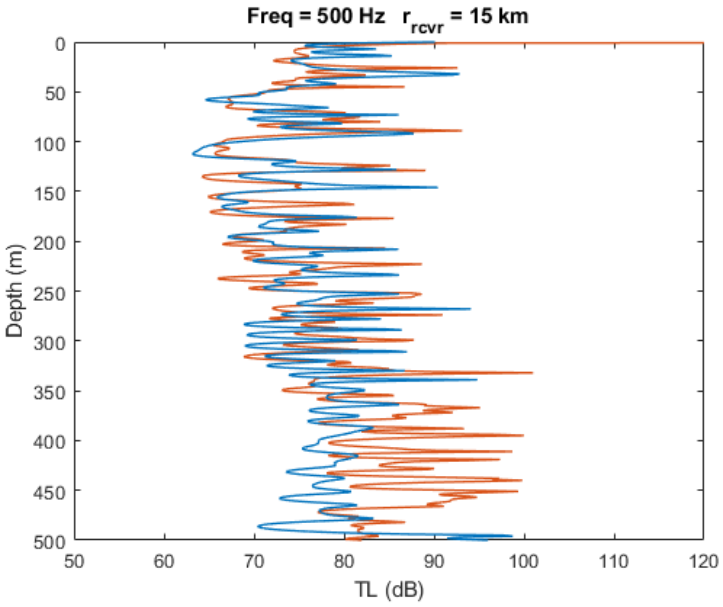

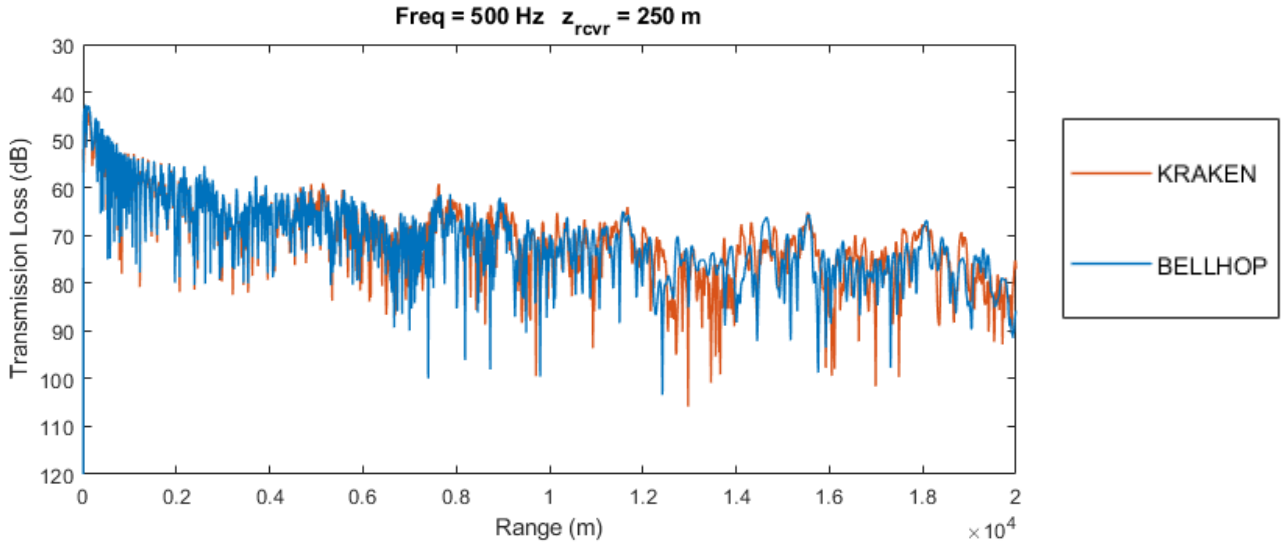

Figures 9-9, 9-10 - TL vs. Range and Depth. Figures 9-11, 9-12 - TL vs. Depth. Figure 9-13 - TL vs. Range.

COMMENTARY ON THE RESULTS OF THE SEAMOUNT CASE

We observe that for the low frequency of 100Hz the field produced by BELLHOP, for areas before the seamount the correspondence between BELLHOP and KRAKEN is satisfactory. Variations in range and depth are well reproduced by both models, although with small differences in the TL values provided. After the seamount, BELLHOP results have some differences when compared to KRAKEN. At 100Hz, the wave diffraction phenomena created after the interaction with the sea mount and the rays seem not to be handled accurately by BELLHOP hence the different coherence patterns at the 100m depth. The region after the mount concerning deep water, presents the same coherence pattern, but a noticeable difference in decibels. The same is visible in the TL vs. range plot, for the region after the mount.

The results are better when shifting to a higher frequency for the upper part of the field. One issue remains though which is obvious at the TL vs. depth plot at 15km range: the “shadow” created by the seamount is not represented accurately by BELLHOP, which predicts higher decibels from KRAKEN. Some phase differences can be observed at the 450m depth mark.

If we focus on the structure of the coherent field, the models appear having obvious deviations at the region after the mount, especially at the low right corner defined by the mount and the bottom. We expect better results from BELLHOP as we go higher in frequency and large number of beams used.

8.2.2 Upslope

This case is an extension of the mount bathymetry by a flat bottom, after $6\ km$, at $250\ m$ depth, which effectively creates an environment of high bottom interactions with the rays. It is interesting to investigate how propagation is handled. First, a simple ray trace:

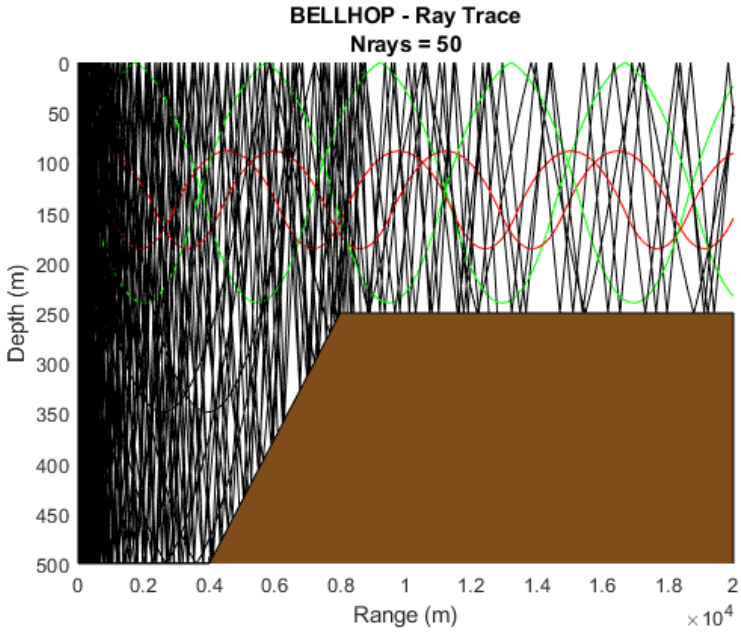

Figure 8-14 Upslope Ray Trace

Similar to the previous case, a single beam is traced to show the interaction with the bottom boundary. This is beam number $101/181$ ($1°$ coverage for the aperture of $180°$) which means it launched at $10°$. We notice how the amplitude of the beam gets weaker in each interaction with the bottom (but not the surface) and also the existence of a focal point:

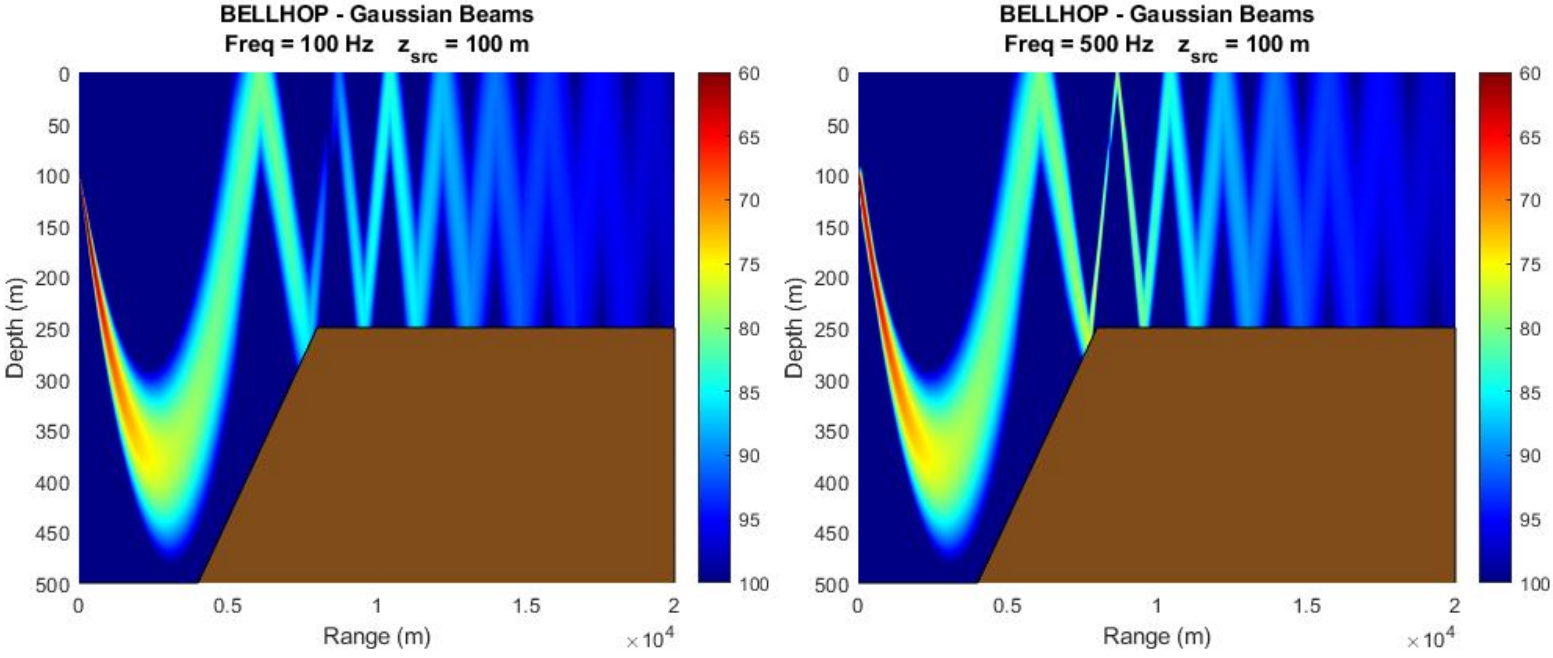

Figure 8-15 Single Beam Trace for the Upslope at 100 Hz and 500 Hz

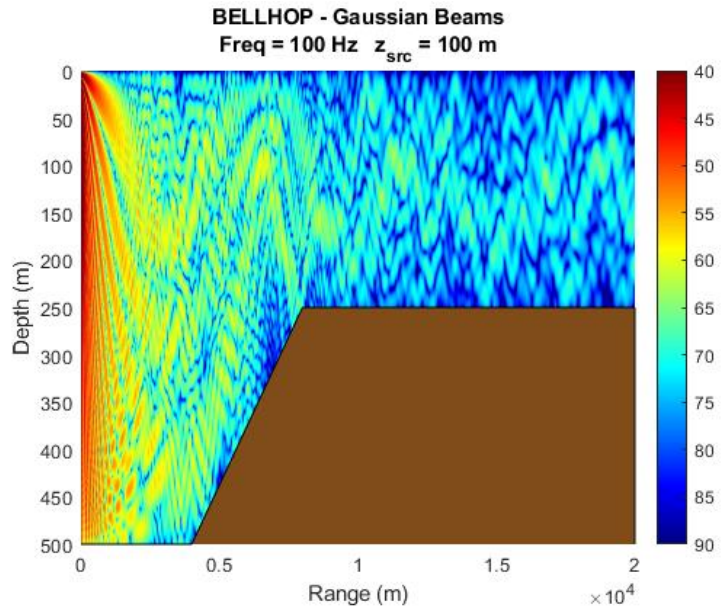

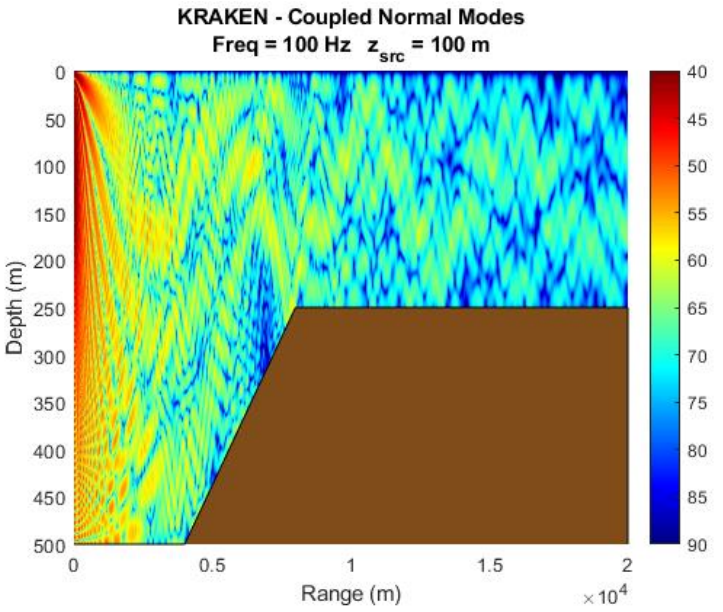

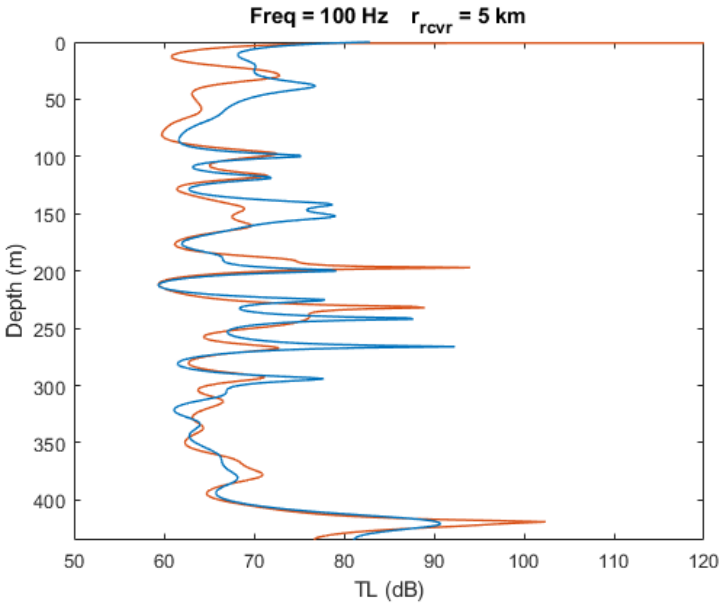

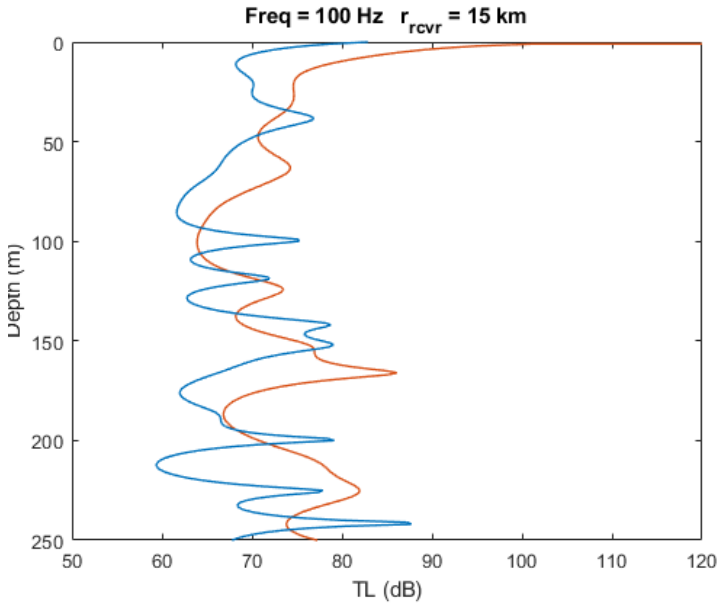

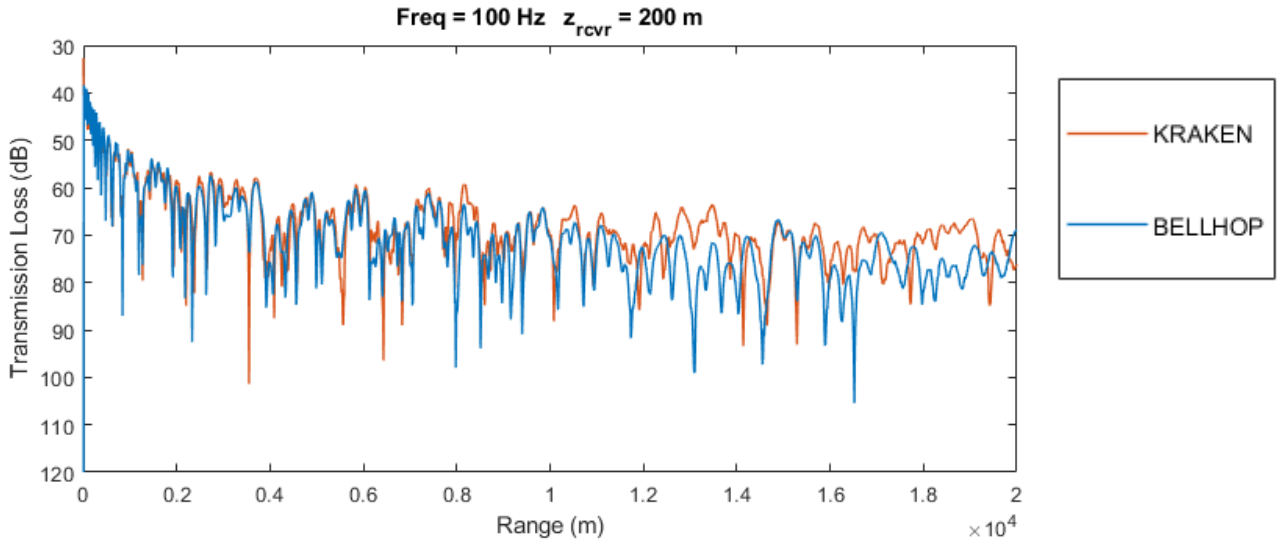

Figures 9-16, 9-17 - TL vs. Range and Depth. Figures 9-18, 9-19 - TL vs. Depth. Figure 9-20 - TL vs. Range.

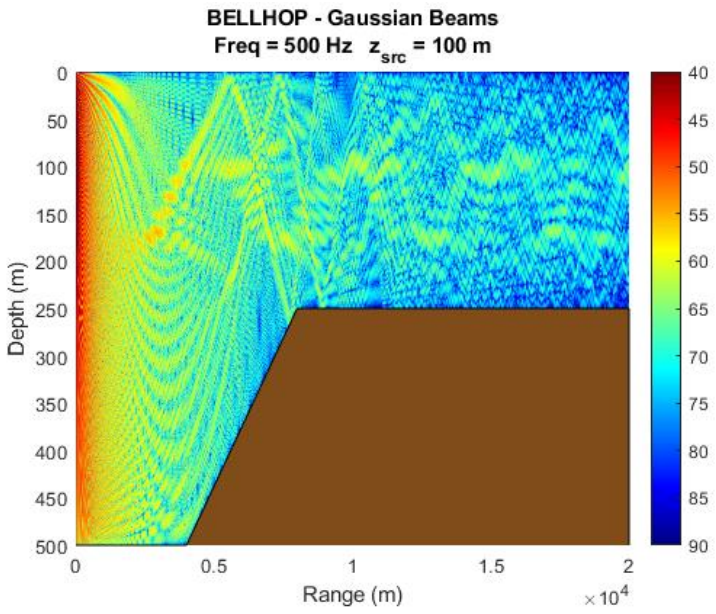

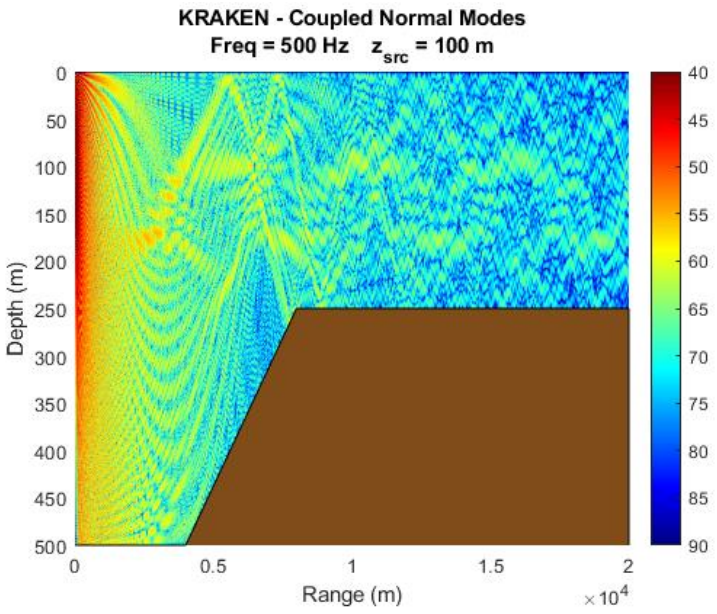

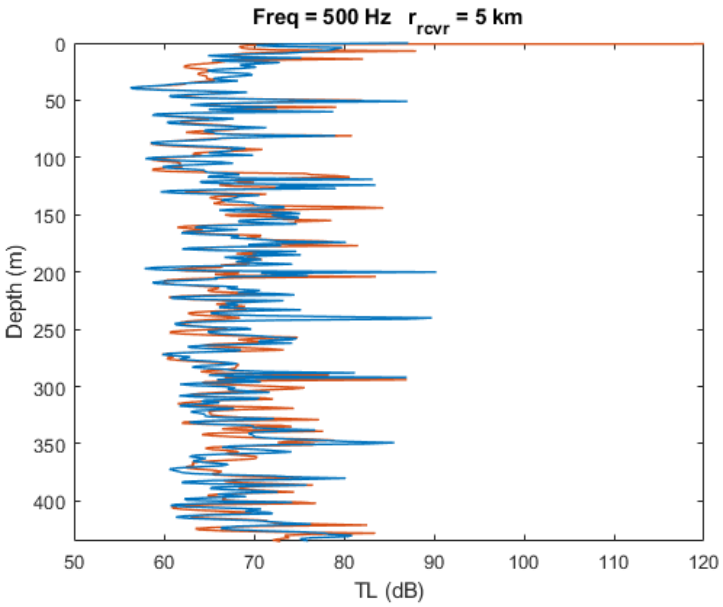

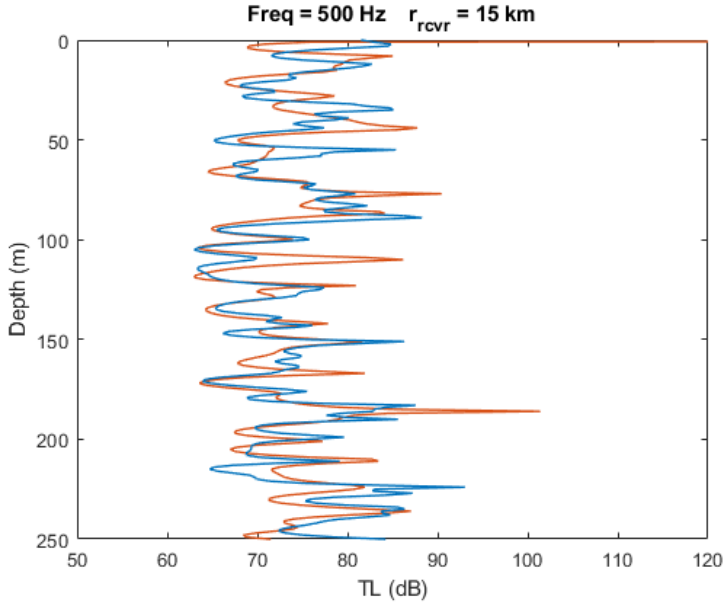

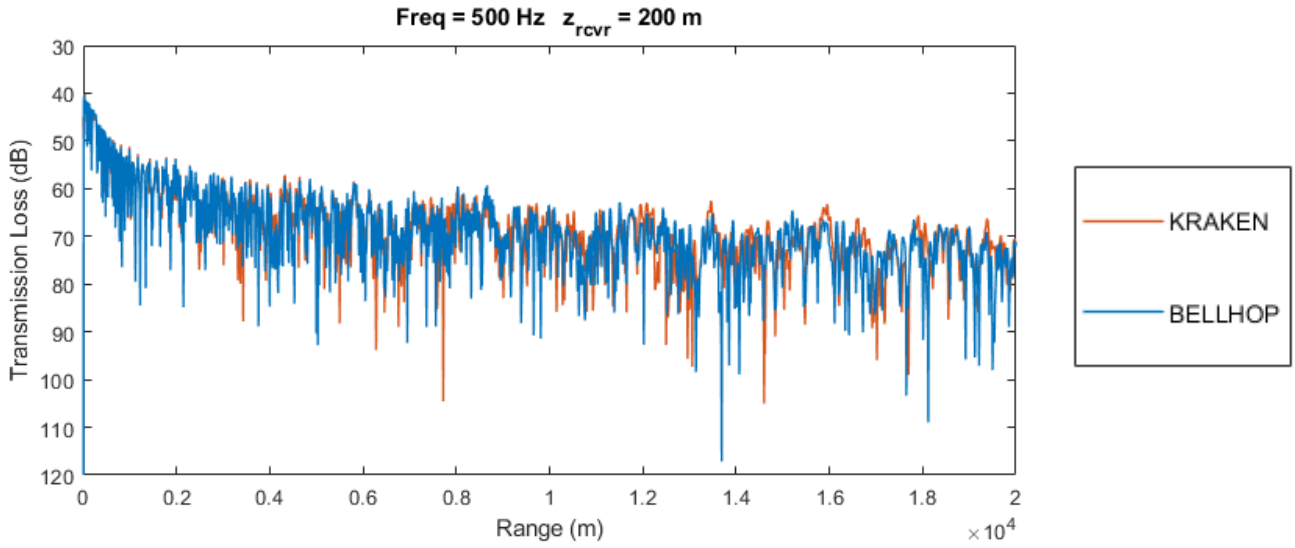

Figures 9-21, 9-22 - TL vs. Range and Depth. Figures 9-23, 9-24 - TL vs. Depth. Figure 9-25 - TL vs. Range.

COMMENTARY ON THE RESULTS OF THE UPSLOPE CASE

At the low frequency of 100Hz, there are some inaccuracies from BELLHOP, especially after the rays interacting with the up sloping bottom. This issue can be attributed to rays hitting in grazing angles the surface and the bottom resulting in phase errors. This is a known issue of BELLHOP and can be minimized by using a large number of rays. The program used 1256 rays at the frequency of 100Hz and 2000 rays for the frequency of 500Hz.

Concerning the Transmission Loss vs. range at 100Hz, we observe that the coherent structure remains the same, although the attenuation of the field is larger for BELLHOP. There is some phase difference at the 17km mark.

The accuracy of BELLHOP is excellent in the high frequency regime, which is expected. BELLHOP automatically uses more rays for higher frequencies which minimize beam widths which means less phase errors. All transmission loss plots show noticeable agreement with the pressure field calculated by KRAKEN.

8.3 Libyan Sea – Northern Crete

(Coordinates of the source – Long: 24.00268, Lat: 33.94094 | Endpoint – Long: 24.3492, Lat: 35.1846)

For the final application, we consider a slice in the Libyan sea, seen in the figure below. The source lies on the red point and represents a commercial ship, thus placed at a logical propeller depth of $10m$, travelling on a well-established route northern of the island of Crete, emitting continuous sound. Two frequencies will be considered at 100 and 500 Hz. The SSP is characteristic of the South East Mediterranean Sea. The range – depth data were acquired from *Salon et al.*(2003) and linearly extrapolated to the max depth of the area.

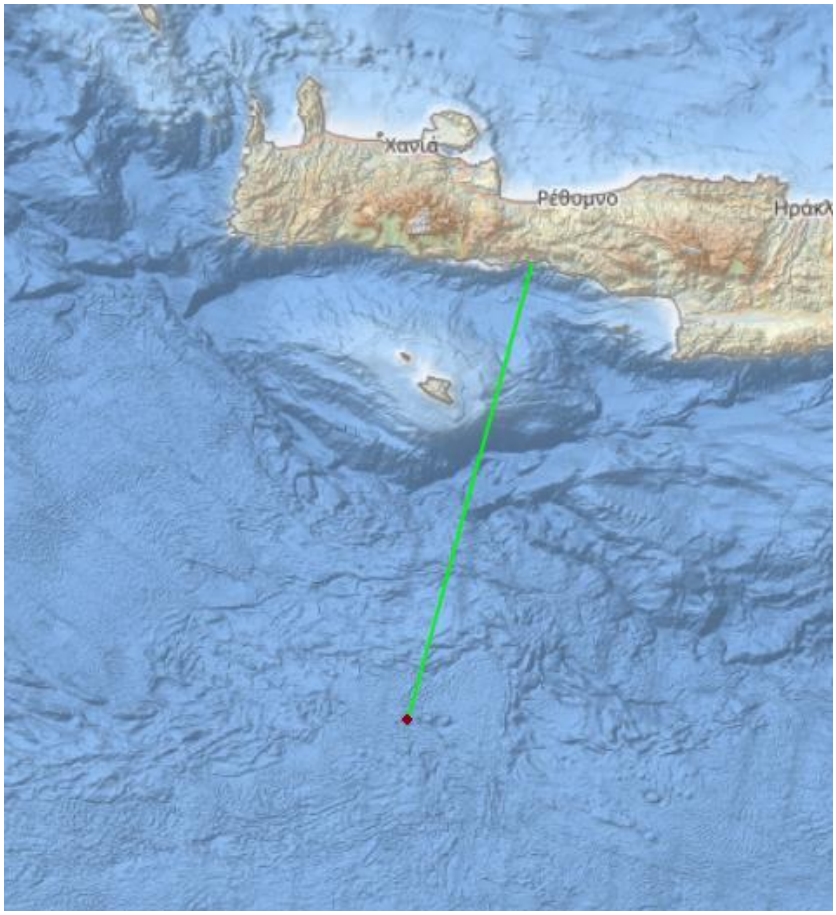

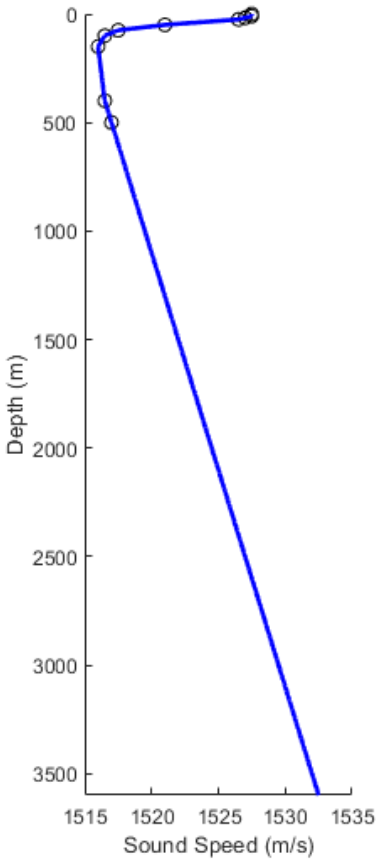

Figure 9-26 – The slice considered in this application. Figure 9-27 – The SSP for the South Easter Mediterranean Sea

This particular slice was chosen because of the complex bathymetry that arises crossing the Hellenic trench at depth $3500m$ and then the immediate elevation at $500m$ close to the island of Gavdos. The properties of the bottom are: speed of compressional waves $c_p = 1650\ {}^{m}/_{s}$, density of $\rho = 1.8\ {}^{gr}/_{m^3}$ and attenuation of $0.5\ {}^{dB}/_{\lambda}$. These properties effectively describe a "soft" bottom.

The bathymetry slice can be divided into three sections. The first section contains some irregular geometry and its endpoint is defined by the sudden plunge, which is the second section. This is the Hellenic Trench, which passes through southern Crete. Last section, is the sudden elevation of $3km$ which happens in the outskirts of the island of Gavdos and reaches the shores of northern Crete.

A ray trace with a few rays was performed to show the characteristic paths:

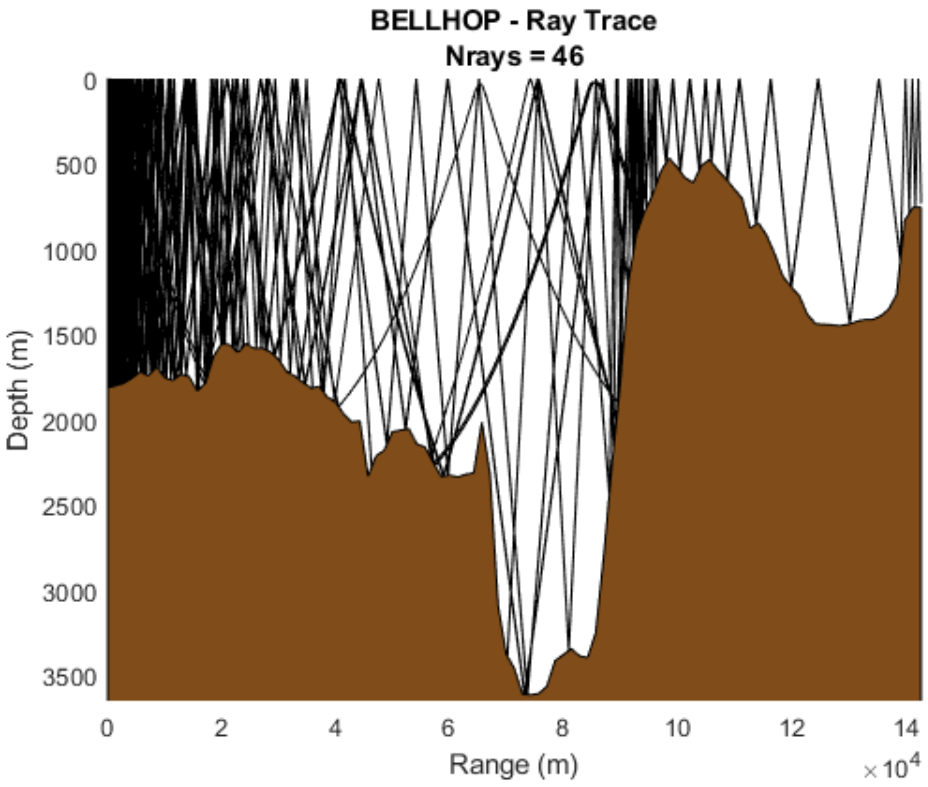

Figure 8-28 A ray trace showing the ray paths

Transmission Loss versus depth plots were calculated at representative ranges of 13, 80 and $130\ km$ for each characteristic section of the slice. Additional plots of Transmission Loss versus range at depths of 200 and $800\ m$ will be calculated to account for observations for energy crossing the $100\ km$ bottleneck and for a fairly deep point.

The results for the two frequencies are presented in the next pages. The colors, representing the different models used, are presented in the legend below:

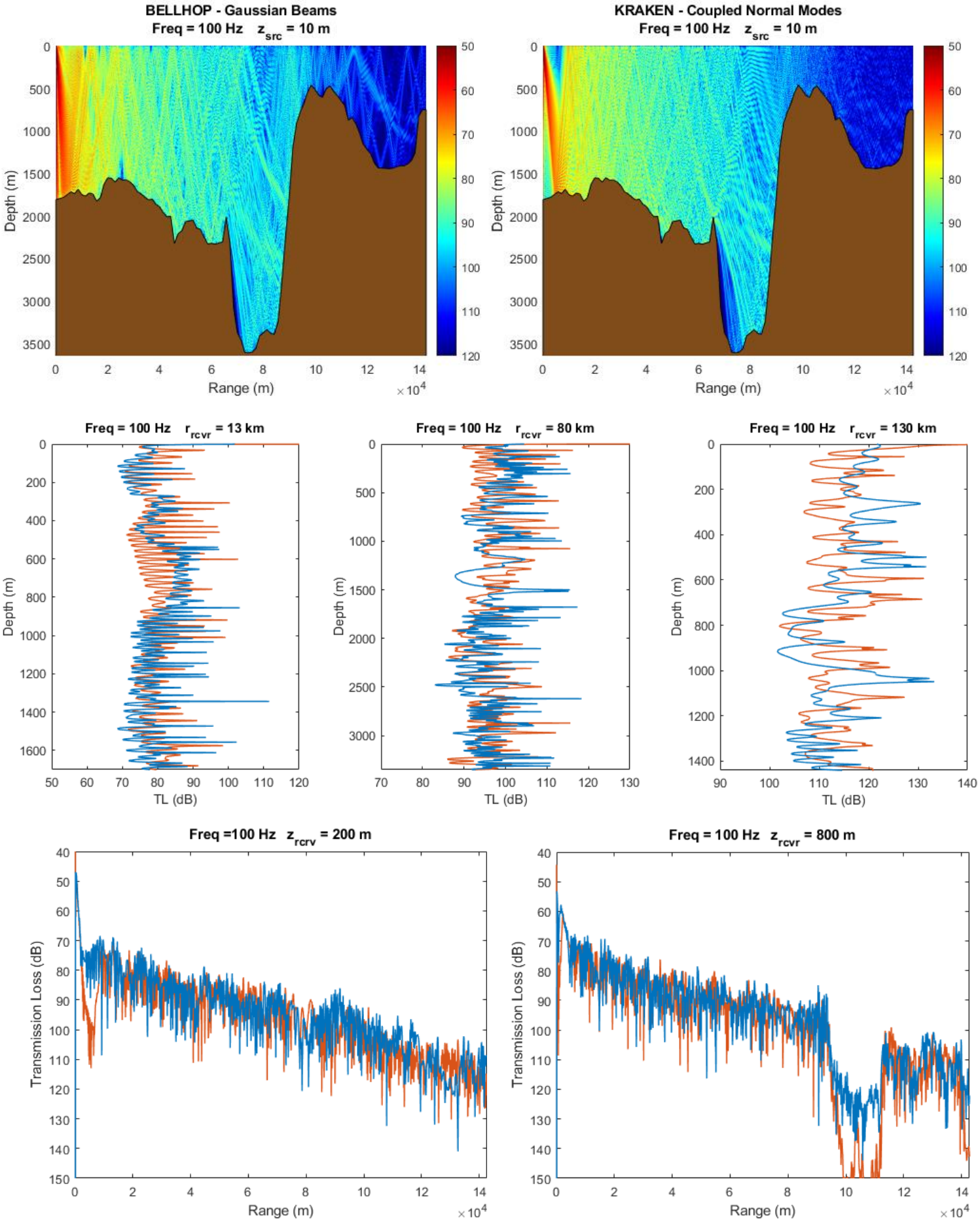

Figures 9-29, 9-30 - TL vs. Range and Depth. Figures 9-31, 9-32,9-33 - TL vs. Depth. Figure 9-34,9-35 - TL vs. Range.

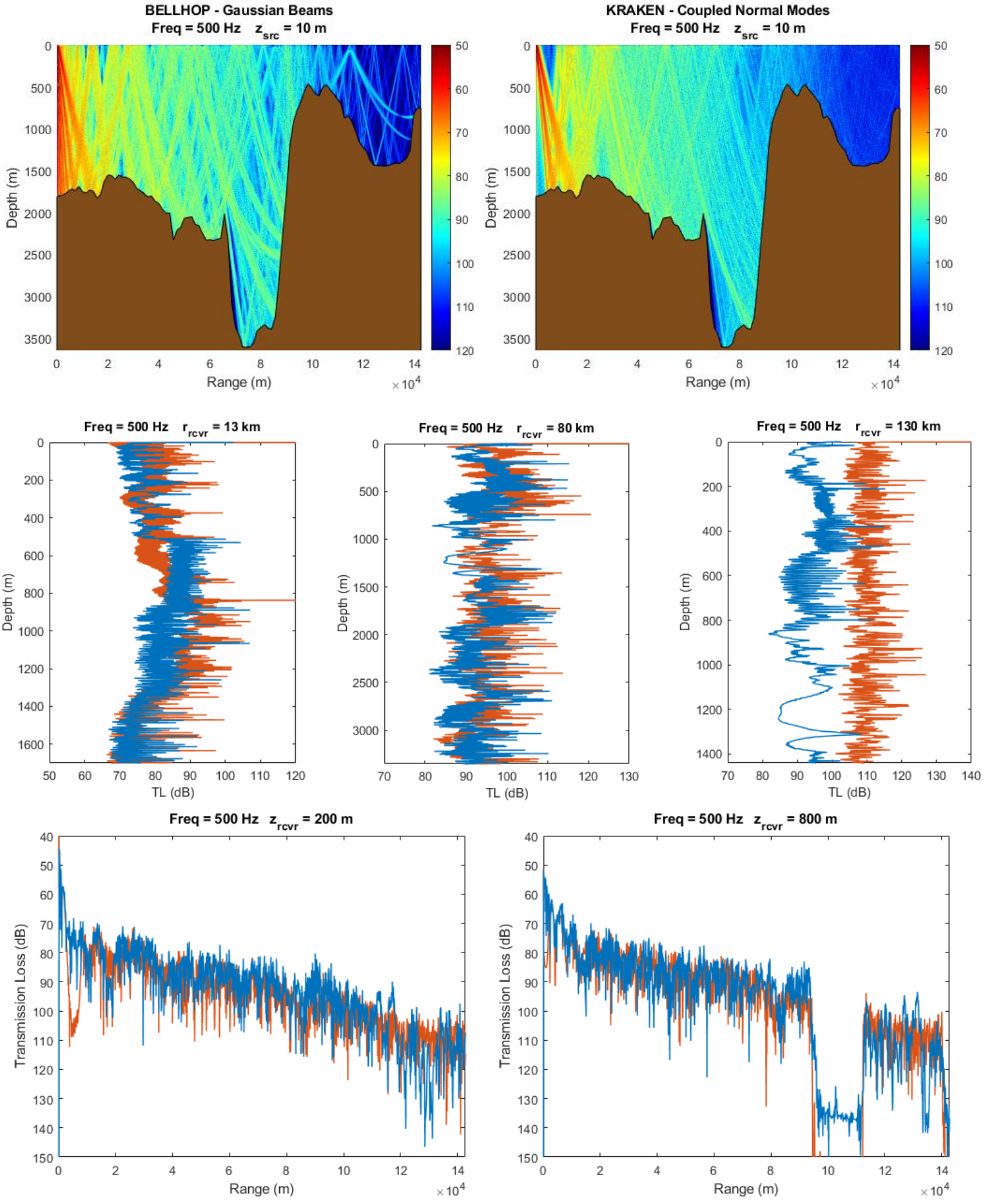

Figures 9-360, 9-37 - TL vs. Range and Depth. Figures 9-38, 9-39,9-40 - TL vs. Depth. Figure 9-41,9-42 - TL vs. Range.

COMMENTARY ON THE RESULTS OF THE NORTHERN CRETE CASE

Initially, we have to stress that this case has a very irregular bathymetry which obviously complicates the results a lot for both models used. However it is a challenging test case.

In general, the pressure field calculated by KRAKEN is considered to be closer to reality as the acoustic energy has a smoothed out distribution. The difference from ray tracing is obvious in the TL vs. range-depth plots, in which high energetic rays are visible. The triangular, quiet zone, predicted by KRAKEN in the vicinity of the source, has been shown to be an artifact of the program due to the very shallow placement of the source and the usage of a second medium to handle range – dependent bathymetry.

The TL vs. range plots are in a fairly good agreement for both receiver depth and frequencies considered, until the third section, after the 100 km bottleneck, in which the models fail to agree. This is also supported by visually inspecting the TL vs. range – depth.

Comparing the acoustic field vs depth plots, we observe that for the case of 13 km in range, large deviations between BELLHOP and KRAKEN are observed for both frequencies between 300 and 800 m depth. The agreement is better for the distance of 80 km for the whole depth and for both frequencies, while for the distance of 130 km, the disagreement among BELLHOP and KRAKEN is much higher especially for the frequency of 500 Hz. We consider that the region after 100 km in range is problematic for BELLHOP. Considering the ray propagation paths shown in Figure 9-28, we conclude that the rays fail to successfully penetrate the shallows and get “clumped” , interacting many times with the bottom, at around 90 km. Some rays are able to get through the bottleneck, but their beamwidth is not large enough to create a realistic representation of the acoustic pressure field and we can clearly see the beam paths.

Finally, even if BELLHOP is inaccurate in TL representation in this scenario, at least at long range prediction in the swallows, it is important to notice that KRAKEN execution time for the high frequency was approximately 4000 seconds but BELLHOP did only 91 seconds. Low execution times is the true power of the gaussian beam method, at the cost of pressure accuracy.

9 Summary

The basic theory of Acoustic Ray Tracing was presented, hopefully in an understandable format and commentary was provided in each step. The content was mostly based in the book of Computational Ocean Acoustics by Jensen et al and the 1987 paper by Porter and Bucker, which are both highly recommended for the interested reader and for the detailed derivation of expressions. The extension of Gaussian Beams is used in many applications and is a very useful understanding for anyone that deals with wave phenomena. Furthermore, I hope I somehow was able to transfer the sense of the approaching and modeling a complex problem which is fascinating, at least. Finally, the key concepts, advantages and disadvantages in theory were presented by running simulations.

In the Seamount case, we explored how the ray solutions have a disadvantage at representing the field after a mount and in the Upslope case, which involved high interaction of rays with the bottom, we concluded that the models are in good agreement.

A real application of a case in Northern Crete was implemented in order to provide a scope on the handling of complex bathymetry and parameters. In conclusion, the Gaussian Beam method is approaching very closely the accurate Normal mode solutions but still lacks the ability to diffuse acoustic energy realistically after a very irregular bathymetry. This is the price for efficient execution times.

The highly complex problem of model agreement and benchmarking is directly related to the geometry of the bathymetry and the dimensions of the waveguide. Furthermore, it is very difficult to address the issue in the same parametric terms, because of the difference in algorithmic structure, which directly relates to the mathematics used for each model. For instance, there is not a direct relation to the “ray step” parameter from BELLHOP to KRAKEN or choosing the same grid decimation for both models does not mean computational equality.

The most lucrative advantage of Beam Tracing is the execution time of the computation, especially for the high frequency spectrum, were normal modes models fail to compute on a reasonable time.

10 Sources and Bibliography

1. Cerveny, V., Popov, M. M., Psencik, I., 1982, *Computation of Wave Fields in inhomogeneous media – Gaussian Beam Approach*, Geophys. J.R. Astron. Soc. 70, 109-128.
2. Duncan, A. J., Maggi, A. L., *A Consistent,* 2006, *User Friendly Interface for Running a Variety of Underwater Acoustic Propagation Codes*, Center for Marine Science and Technology, Curtin university of Technology, Proceedings of ACOUSTICS.
3. Etter, P. C., *Underwater Acoustic Modeling and Simulation*, 3rd edn., CRC Press, 2013.
4. Hovem, M. Jens, Ray Trace Modeling of Underwater Sound
5. Jensen, F. B., Kuperman, W. A., Porter, M. B., and H. Schmidt, 2011, *Computational Ocean Acoustics,* 2nd edn., Springer
6. Ocean Acoustic Library – BELLHOP – http://oalib.hlsresearch.com/Rays/index.html
7. Paul A. Baxley and H. P. Bucker, *2000, Proceedings of the Fifth European Conference on Underwater Acoustics, ECUA*.
8. Porter, M. B. and H. P. Bucker, 1987, *Gaussian beam tracing for computing ocean acoustic fields, J. Acoust. Soc. Am.,* 82 (4), 1349-1359
9. Porter, M. B., 2001, *The KRAKEN normal mode program*, SACLANT Undersea Research Centre
10. Porter, M. B., 2011, *The BELLHOP Manual and User's Guide: Preliminary Draft,* Heat, Light, and Sound Research, Inc., La Jolla, CA, USA
11. Rodriguez, C. O., 2008, *General Description of the BELLHOP Ray Tracing Program*.
12. S. Salon, A. Crise, P. Picco, E. de Marinis, and O. Gasparini, *Sound Speed In The Mediterranean Sea: An Analysis From A Climatological Data Set*, *Annales Geophysicae (2003) 21: 833–846c European Geosciences Union*
13. Taroudakis, M. , *Introduction to Ocean Acoustics (Εισαγωγή στην Ακουστική Ωκεανογραφία) – Class Notes (Ray and Sonar Theory)*